Ocean Engineering 260 (2022) 111964

Contents lists available at ScienceDirect

Ocean Engineering

journal homepage: www.elsevier.com/locate/oceaneng

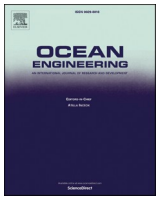

Prediction of potential net panel selectivity in mesopelagic trawls

Eduardo Grimaldo [a,b,*,1], Bent Herrmann [a,b,c,1], Jure Brčić [d,1], Kristine Cerbule [a,b,1], Jesse Brinkhof [a,b], Leif Grimsmo [a], Nadine Jacques [b]

[a] Department of Fishing Gear Technology, SINTEF Ocean, Trondheim, Norway
[b] UiT the Arctic University of Norway, Tromsø, Norway
[c] DTU Aqua, Denmark Technical University, Hirtshals, Denmark
[d] University of Split, Croatia

ARTICLE INFO

Keywords:
Mesopelagic trawl
Trawl design
Mesh opening
Tapering angle
Mesopelagic fish
Selectivity
Catch efficiency

ABSTRACT

The growing interest in harvesting mesopelagic fish species has increased the need for knowledge about how trawls should be designed for optimizing the catch efficiency of these resources. Since the net herding efficiency for small mesopelagic fish species is unknown, trawls targeting these species need to consider the potential net panel selectivity along the entire trawl body. Therefore, trawl engineers and net makers who design trawls for harvesting mesopelagic species need to know which design parameters, such as mesh size, mesh opening angles, and trawl tapering angles, can be used along the trawl body to avoid potential net panel selectivity, thus maximizing catch efficiency. This study addresses these knowledge gaps using an approach based on laboratory experiments with mesopelagic fish and a simulation model that can help in predicting the potential net panel selectivity. Three trawl designs that have been used in experimental fisheries in the Northeast Atlantic are investigated in this study. Two of them (trawl 1 and trawl 2) had small-mesh liners in the belly and extension piece while the third trawl didn't. The simulation model shows that trawls with small-mesh liners in the belly and extension piece reduces panel selectivity and can increase catch efficiency.

1. Introduction

Global mesopelagic stock estimates indicate a potential biomass that goes far beyond any other commercial fishing resources, ranging from 1 billion tons (Gjøsaeter and Kawaguchi, 1980) to 11–15 billion tons (Irigoien et al., 2014). Since the 1970's, mesopelagic resources around the world have been subject to large-scale fisheries development (Pauly et al., 2021). However, catch rates from several trial fisheries do not correspond to global biomass estimates (Boyra et al., 2013; Prellezo, 2019; Bjordal and Thorvaldsen, 2020; Grimaldo et al., 2020), and none of the commercial attempts have proven to be viable (FAO, 1997; Standal and Grimaldo, 2020). Instead, the rather disappointing results have revealed major knowledge gaps about mesopelagic fish stocks, their position in the ecosystem, and technological developments for cost efficient harvesting (St. John et al., 2016). Despite these uncertainties, mesopelagic species are still regarded as a potential source for a new large-scale pelagic fishery (St. John et al., 2016; Hidalgo and Browman, 2019). Therefore, optimal mesopelagic trawl designs are needed to target mesopelagic species.

There have been several previous commercial attempts to harvest mesopelagic fish resources. For example, a Soviet Union (USSR) fishery for blue lantern fish *Diaphus coeruleus* and Nichol's lanternfish *Gymnoscopelus nicholski* was established in the Southwest Indian Ocean and Southern Atlantic in 1977. The catch rates by former USSR countries reached 51680 tons in 1992, after which the fishery ceased (FAO, 1997; Pauly et al., 2021). The Icelandic pelagic trawlers caught 46000 and 18000 tons of Muller's pearlsides (*Maurolicus muelleri*) in 2009 and 2010, respectively, taking advantage of the availability of this mesopelagic fish species in Icelandic waters in those years (Sigurdsson, 2017; Pauly et al., 2021). In Norway, some pelagic trawlers conducted commercial trial-fisheries from 2016 to 2020 (Bjordal and Thorvaldsen, 2020; Grimaldo et al., 2020). Results from these trials indicate considerable variations in terms of mesopelagic catch rates, as well as catch composition and amounts of bycatch. In 2019, commercial trial-fisheries within Norway's economic exclusive zone (EEZ) landed a total of 1693 tons of mesopelagic species, of which 1223 tons were Muller's

* Corresponding author. Department of Fishing Gear Technology, SINTEF Ocean, Trondheim, Norway.
E-mail address: eduardo.grimaldo@sintef.no (E. Grimaldo).
[1] Equal authorship.

https://doi.org/10.1016/j.oceaneng.2022.111964
Received 9 February 2022; Received in revised form 25 May 2022; Accepted 8 July 2022
Available online 17 July 2022
0029-8018/© 2022 The Authors. Published by Elsevier Ltd. This is an open access article under the CC BY license (http://creativecommons.org/licenses/by/4.0/).

pearlsides, with a significant bycatch of krill *Meganyctiphanes norvegica* (Bjordal and Thorvaldsen, 2020).

The overall size of a mesopelagic trawl largely determines its ability to catch swimming organisms entering the trawl opening. This must be traded off against mesh size, which determines the retention of small organisms. Fine-meshed trawls cannot be towed at speeds high enough to capture species that show avoidance behaviour (Heino et al., 2011). Catchability is thus defined as the expected ratio of catch in numbers with respect to the organisms entering the trawl. In general, catchability is determined by both the properties of the trawl (i.e., mesh size, tapering angle, mesh opening angles), the characteristics of the organisms encountered (i.e., swimming speed, endurance), and the interactions between them (i.e., herding behaviour). Heino et al. (2011) described four major factors that are expected to cause systematic differences in the catchability of the trawls. First, the *filtered volume*, which is proportional to the mouth area of the trawl. However, strict proportionality between the filtered volume and catches is expected only when there is no avoidance and all individuals in the filtered volume are retained by the trawl (Barkley, 1972). Second, *fish avoidance behaviour,* which makes it necessary to increase the diameter of a trawl and the towing speed to increase catchability. Third, *retention through mesh selection,* which depends on the mesh size relative to the size of individuals, as well as their body shape and form (Herrmann et al., 2012; Cuende et al., 2020). Fourth, the *herding effect* in pelagic trawls, in which catchability is based not only on the filtering effect but also on the behavioural response of fish towards the trawl panels. Fish inside the trawl try to avoid the meshes and do not swim through them but are instead herded into the middle of the trawl, eventually encountering meshes that are small enough for retention (Lee et al., 1996; Valdemarsen, 2001).

Like krill trawls, mesopelagic trawls are also usually low tapered constructions where small-mesh net panels, herein called small-mesh liners, are fitted inside the trawl body and the codend to reduce the loss of catch through the mesh. Small-mesh liners are now widely used in krill trawls and cover various proportions of the trawl body length from 0% (without liner) to 100% (covering the entire trawl body and codend) (Xu et al., 2015; Li et al., 2017). These liners are designed as a series of overlapping cones, resulting in a wave motion that gently ripples with the flow of water and prevents small organisms from become enmeshed (Underwood et al., 2016; Zhou et al., 2016). Although the introduction of small-mesh liner trawls resulted in great increases in catch, the wave motion produced towards the codend results in higher hydrodynamic drag of the trawl system, reduced spread and mouth opening, and lower size selectivity (Xu et al., 2015). In Norway, three different types of pelagic trawls have been used to catch mesopelagic fish species since 2016, two of them with small-mesh liners in the belly, extension piece and codend, and one of them with small-mesh liners only in the codend. Under commercial fishing, these mesopelagic trawls have shown different catch efficiencies, most likely due to different selection properties in relation to species and differences in fish behaviour.

Trawls with small-mesh liners caught significantly more krill than trawls without liners, which caught cleaner catches of Muller's pearlsides (Grimaldo et al., 2020; Bjordal and Thorvaldsen, 2020). Therefore, understanding the effects of trawl design features (i.e., tapering angles, mesh sizes and mesh opening angles) on the size selection of mesopelagic species (fish and crustaceans, i.e., krill) is important for identifying the technical measures required to target these species. Size selectivity and bycatch reduction represent the ability of a given trawl to catch different sizes of a targeted species and it is a key parameter for the development of sustainable fishery management (Wileman et al., 1996). The selectivity of a net panel not only depends on the mesh size, mesh opening, and the tapering angle (the angle in which the fish meets the net panel), but also on the morphology and behaviour of a given target species (Herrmann et al., 2009; Brčić et al., 2018; Santos et al., 2018). Some mesopelagic fish, like Muller's pearlsides are able to avoid (or seek) net panels actively, while others, i.e., glacier lantern fish (*Benthosema glaciale*), are passively sorted and their selectivity depends largely on mesh size, mesh shape, and tapering angles (Grimaldo et al., 2020). Size selection resembles a sieving process in which individuals may contact the netting multiple times following a random angle trajectory for each of the contacts (Polet, 2000; Herrmann et al., 2018).

Size selectivity studies in trawls have traditionally been made by conducting a series of sea trails. Sea trials are economically costly and time consuming, and there is therefore a limit to the number of different gear designs that can be tested. Mesopelagic trawls are made of different mesh sizes along the belly, extension, and codend. They often have different tapering angles which lead to changes in mesh opening angles along the trawl body. Depending on the fish species, selection processes in mesopelagic trawls can also occur along the entire trawl body before fish enter the codend (Bjordal and Thorvaldsen, 2020).

Therefore, we combined trawl design features, trawl operational measurements, and laboratory fall-through experiments for two of the most common target fish species in mesopelagic trawling (Muller's pearlside and glacier lanternfish) to model the effect of mesh size, tapering angle, and mesh opening angle on the size selectivity of three mesopelagic trawl designs that have been used by Norwegian commercial vessels (pelagic trawlers) since 2016.

2. Materials and methods

2.1. Trawl designs

Three mesopelagic trawls were used by the 68 m long pelagic trawler "MS Birkeland" to conduct experimental fishery of mesopelagic species in the Northeast Atlantic during 2016–2018 and Norwegian EEZ during 2020 as follows:

- Trawl 1: Egersund-1200 m trawl (1200 m stretched mouth circumference) (Supporting file 1),
- Trawl 2: Egersund-800 m trawl (800 m stretched mouth circumference) (Supporting file 2),
- Trawl 3: Thybøron-1226 m (1226 m stretched mouth circumference) (Supporting file 3).

In addition, Trawl 3 was also used by the 64 m long pelagic trawler "MS Ligrunn" to conduct experimental fishery of mesopelagic species in the Norwegian EEZ during 2018–2020.

A series of 40, 30, 24, and 20 mm small-meshed liners were attached inside the trawl belly and extension piece of Trawl 1 and Trawl 2 to avoid the escape of mesopelagic fish and increase catch efficiency. The liner mesh sizes were chosen as a compromise between maximizing the trawl catch area and reducing the total drag of the trawl. The liners are constructed as a series of overlapping cones, resulting in a wave movement that undulates gently with the flow of water and prevents small organisms from becoming enmeshed (Fig. 1). Trawl 3 did not have liners and the meshes in the belly were gradually reduced from 3200 mm to 30 mm in the extension piece. The same design of a 93 m codend, blinded with small-mesh liners of 16 and 12-mm mesh size, was used by all trawls. All trawls were small-scale tested (Trawls 1 and 3 were scaled at 1:50 while Trawl 2 was scaled at 1:40) in a flume tank in Hirtshals, Denmark in October and November 2016, and the final designs were adjusted before full-scale construction. The total drag (mean ± standard deviation) of Trawl 1, 2, and 3 at 2.0 knots was 412370 ± 1176, 431493 ± 1275, and 321658 ± 1177 N, respectively, while at 2.5 knots it was 535443 ± 1079, 619780 ± 1177, and 358923 ± 1079 N, respectively.

While only Trawl 3 was used by MS Ligrunn to conduct experimental fishery off the western coast of Norway (60°51′ N 03°41′ E) in 2019, all trawls were used by "MS Birkeland" in the same area in 2020. A Simrad trawl sonar, type FS20/25, 90 kHz horizontal, and 120 kHz vertical sonar heads (Konsberg Maritime AS, Norway), helped in monitoring the geometry of the trawl mouth cross-section and measuring the trawl height and width. In addition, trawl height was monitored with a

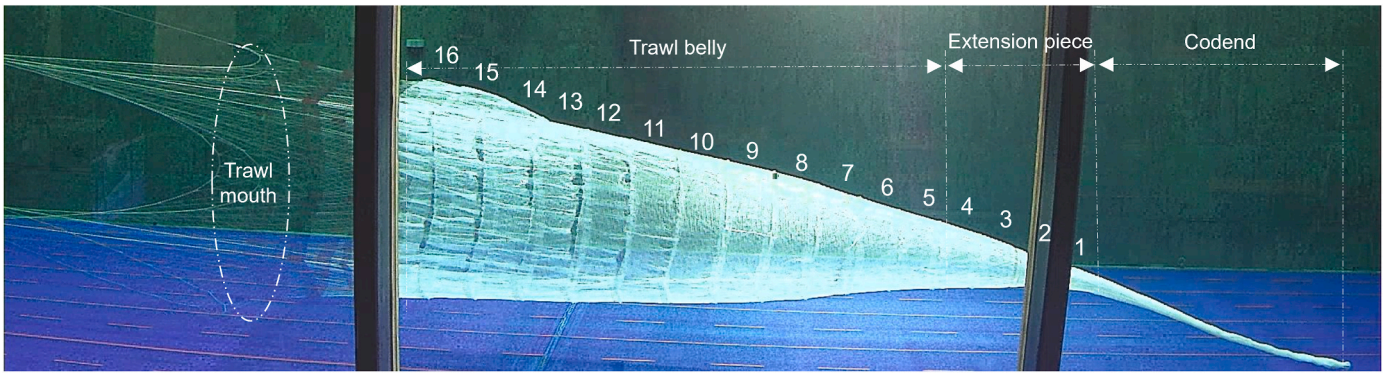

Fig. 1. Image showing the small-scale testing of Trawl 2 in the flume tank. The small-meshed liners are numbered, starting from the trawl's extension piece (liners 1–16). (See supporting file 2 for details).

Scanmar trawl sonde (97 kHz) (Scanmar AS, Norway), which was attached to the top panel of the trawl in different trawl sections along the trawl's belly and extension piece. The towing speed varied between 2.2 and 2.4 knots. Underwater video was recorded to study fish behaviour relative to the trawl, small-mesh liners, and codend. We used two or four GoPro Hero4 Black edition cameras and red/infrared (620–630 nm) lights to provide adequate illumination. These devices were attached inside and outside the top panel of the trawl at different locations along the trawl body, extension piece, and codend.

2.2. Estimation of trawl parameters under operation

Since the three trawls differ significantly in design, it was expected that parameters like the trawl operational circumference (*C*), mesh sizes (*MS*), tapering angles (θ), hanging ratios (*E*), and mesh openings angles (*OA*) would have different effects on the selectivity and catch efficiency of the trawls. Actual measurements of trawl height and width were collected using the trawl sonar and the trawl sonde and were fitted to the equation of an ellipse that enable the estimation of *C* in each section of the trawl. Then using the trawl drawings, we estimated *C*, θ, *E*, and *OA* of each of the panels along the trawl belly, trawl extension piece, and codend.

θ of each trawl section was estimated as $\theta = arctan\,(a/b)$, where $tan\,\theta$ equals the angle between the netting and the incoming flow direction. D_1 and D_2 are the large and small diameter of one trawl section under operation, respectively, $a = (D_1\text{-}D_2)/2$, b is the length of the section multiplied by the vertical hanging ratio E_2 (Fig. 2). The actual shape of meshes was determined by estimating *E* using the equations described by Fridman (1986), where the horizontal hanging ratio E_1 is the relationship between the hung length of the netting and the stretched length of the netting, and $E_2 = (1 - E_1)^{1/2}$. Based on E_1 and the length of the mesh bar (l), we estimated *OA* (2β) using the following equation:

$$\beta = arcsin\,((\mathrm{E}_1 \times l)/l) = arcsin\,(E_1) \quad (1)$$

For Trawl 1 and 2, parameters were estimated for the outer netting and small-mesh liners. For Trawl 3, which did not have small-mesh liners, these parameters were only estimated for the outer netting.

2.3. Prediction of the potential length dependent loss of Muller's pearlside and glacier lanternfish through mesh selection in mesopelagic trawls

Prediction of potential length dependent fish loss through mesh selection as a consequence of *MS*, θ, and *OA* was investigated following five key steps:

In *step 1,* Muller's pearlsides were collected in July 2019 on board the pelagic trawler "Birkeland" off the western coast of Norway (60°51′ N 03°41′ E) using Trawl 3. Samples of glacier lantern fish were collected in 2019, off the coast northern Norway (69°32′ N and 18°02′ E), on board the research vessel "Helmer Hanssen" using a standard Campelen sampling bottom trawl. Samples were selected to cover wide range of length classes.

In *step 2*, fall-through experiments were conducted (Herrmann et al., 2013; Herrmann et al., 2021) to test which length sizes of fish can geometrically pass through mesh templates with different *MS* and *OA*. The length of 311 Muller's pearlsides and 71 glacier lanternfish was measured to the nearest mm, the fish were then presented head first, and optimally oriented to 54 different mesh templates. Optimal orientation implies that the fish is positioned in a way that maximizes its chance of passing through each mesh template (Fig. 3). The mesh templates, perforated in 3 mm thick nylon plates (Fig. 3), included six different *MSs*: 6 mm, 12 mm, 16 mm, 20 mm, 24 mm, and 30 mm. Some of these *MSs* corresponded to the *MS* of the small-mesh liners used in the trawls. For each *MS* there were nine different *OAs*: 10°, 20°, 30°, 40°, 50°, 60°,

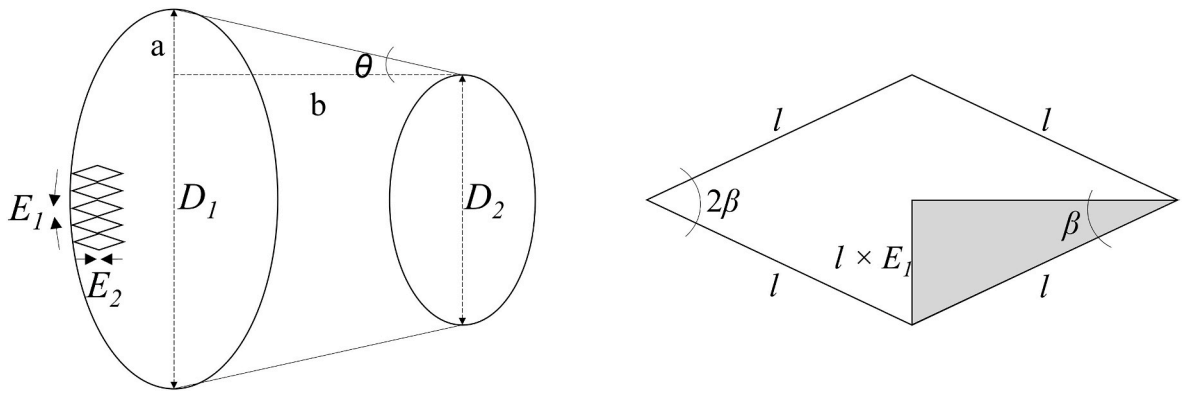

Fig. 2. Estimation of the tapering angle θ, horizontal and vertical hanging ratios, E_1 and E_2, and opening angle $OA = 2\beta$ in one section of the trawl.

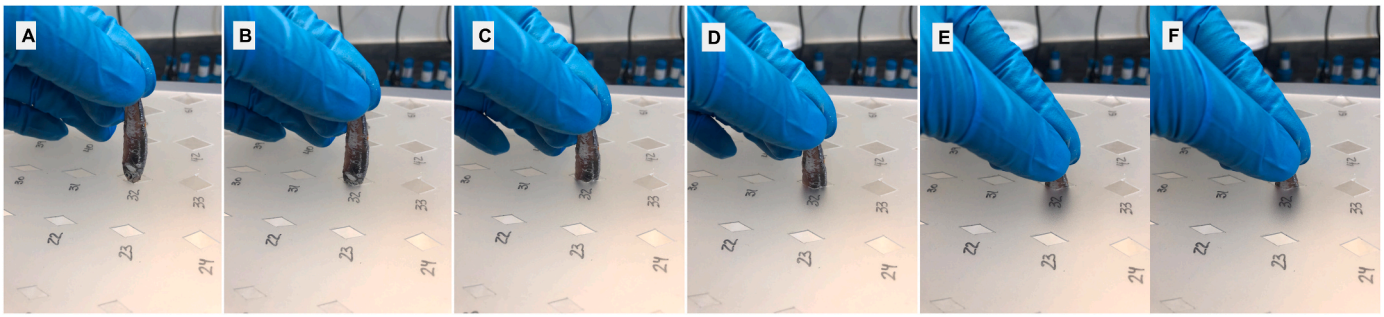

Fig. 3. Images A–E show the fall-through experiment with an optimally oriented Muller's pearlside successfully passing through a mesh template.

70°, 80°, and 90°. The only force acting on the fish was gravity (Fig. 3).

In *step 3*, successful and unsuccessful passage was recorded for each mesh template and each fish. The data were then treated as covered-codend data (Wileman et al., 1996), where each fish that passed through the mesh template was considered to end up in the cover, while the others were considered to be retained in the codend. The fall through data for each mesh template separately was sorted into length classes (l) that contain results for all fish within a specific length interval of 1.0 mm. For each length class the number of fish that passed through (ncc_l) and those that didn't (nc_l) are counted. The experimental retention probability r_l at each length class l is obtained by the following equation:

$$r_l = \frac{nc_l}{nc_l + ncc_l} \tag{2}$$

The following logit size selection model was then fitted to each fall-through dataset to obtain a size selectivity curve for each mesh template:

$$r(l, l50, SR) = \frac{e^{\frac{\ln(9)}{SR}\times(l-l50)}}{1+e^{\frac{\ln(9)}{SR}\times(l-l50)}} \tag{3}$$

The l in Eq. (3) represents fish total length, $l50$ is the length at which the fish has 50% probability of being retained in the codend, SR is the selection range, which is equivalent to $l75 - l25$ (Fig. 4).

When fitting selection curves to covered-codend data, the logit model is commonly used. The functional form for this model is presented above in Eq. (3) with the model parameters estimated using a Maximum Likelihood Estimation (MLE). The model parameters ($l50$ *and* SR) are estimated for each template separately. The values for $l50$ and SR are obtained by minimizing the following expression which corresponds to maximizing the likelihood for the observed fall-through data:

$$-\sum_l \{nc_l \times \ln(r(l, l50, SR)) + ncc_l \times \ln(1.0 - r(l,\ l50,\ SR))\} \tag{4}$$

The estimated $l50$ and SR values, their covariance matrix, together with the corresponding MS and OA value for each mesh template were then used to establish the following predictive size selection model:

$$l50 = \alpha_1 \times MS \times OA + \alpha_2 \times MS \times OA^2 + \alpha_3 \times MS \times OA^3 + \alpha_4 \times MS \times OA^4$$

$$SR = \beta_1 \times MS \times OA + \beta_2 \times MS \times OA^2 + \beta_3 \times MS \times OA^3 + \beta_4 \times MS \times OA^4 \tag{5}$$

The $\alpha_1 \ldots \alpha_4$ and $\beta_1 \ldots \beta_4$ in Eq. (5) are the model parameters that need to be estimated. All simpler sub-models obtained by leaving out one or more terms at a time from Eq. (5) were also considered for predicting $l50$ and SR following the procedure described in Brčić et al. (2018) and Herrmann et al. (2021). From the total of 256 models for each species, the model with the lowest AICc value was chosen as the best model. AICc is the Akaike Information Criteria (AIC) (Akaike, 1974) with a correction for finite sample size (Burnham and Anderson, 2002).

In *step 4,* the best model for each species was applied to predict $l50$ and SR values for each mesh template used in the fall-through experiment. To check for model self-consistency, the model predictions were plotted together with their respective 95% confidence intervals against the $l50$ and SR values estimated by fitting a logit size selection model Eq. (3) to each fall-through dataset. If the predictions represented the trends of the fall-through data well, they were summarized in an isoline graph (lines with equal $l50$ values) called the design guides. The design guides depict how $l50$ values vary with the change in MS and OA (Brčić et al., 2018; Herrmann et al., 2021).

While performing the fall-through experiments, we assumed that fish were optimally oriented when contacting the mesh. However, during fishing, meshes are never perpendicular to the natural swimming path of the fish (Briggs, 1992; Briggs and Robertson, 1993) and fish often meet the meshes at a suboptimal angle (Fig. 5). Fish that are good swimmers and are not exhausted from swimming in front of the trawl opening prior

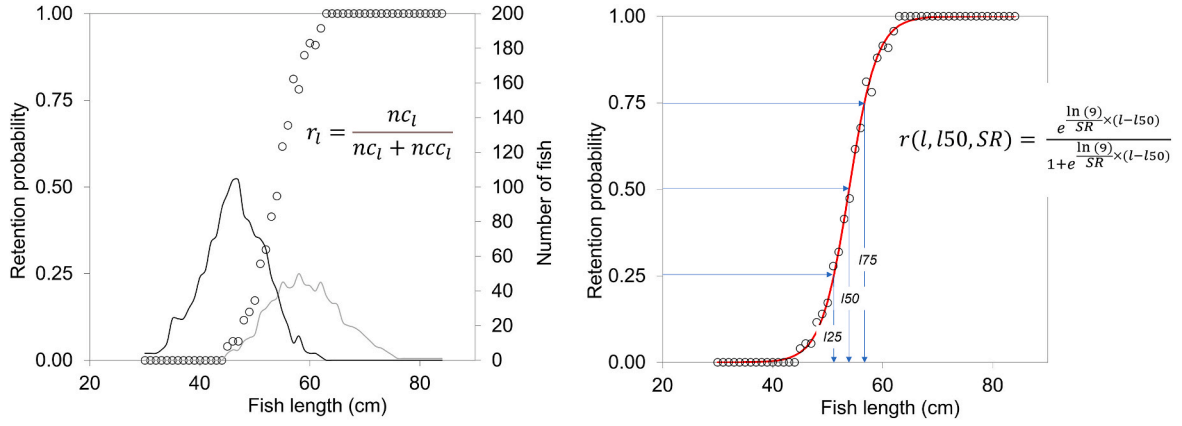

Fig. 4. To the left is the estimation of the retention probability (circles) based on the length frequency distribution of fish that passed through the meshes (black line) and fish that didn't (grey line). To the right is the fit of the logic model showing the $l50$ and the SR (=$l75$-$l25$).

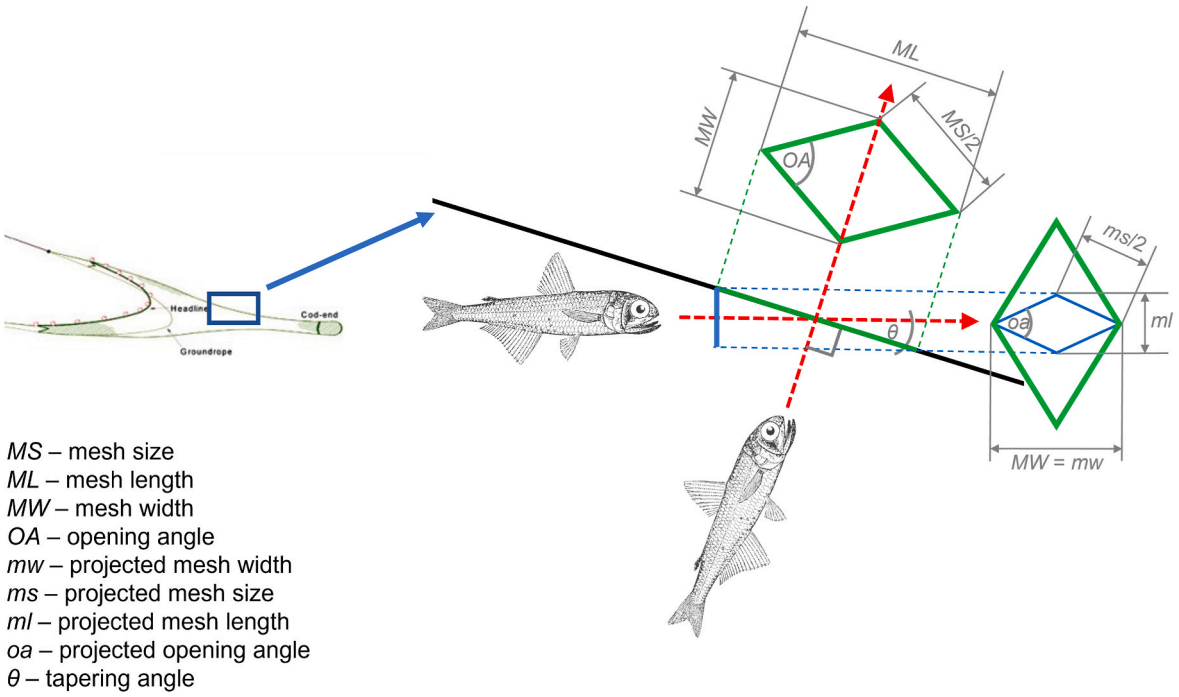

Fig. 5. Illustration showing available mesh area as fish meet the mesh at optimal (90°, green) and suboptimal (blue) angles. (For interpretation of the references to colour in this figure legend, the reader is referred to the Web version of this article.)

to entering it, are able to actively change their position to obtain optimal orientation and maximize their chance of escape. Muller's pearlside and glacier lantern fish grow up to 8 cm (Muus and Nielsen, 1999) and 10 cm (Hulley, 1990), respectively. Therefore, we assumed they encounter trawl meshes at a suboptimal angle (equal to, or close to the tapering angle of the section of the trawl where they encounter the meshes), and, due to limited swimming ability, do not have enough strength to overcome the strong water flow inside the gear to actively change their position to obtain an optimal orientation and maximize the chance of escape. As the tapering angle decreases towards the codend, the projection of the meshes becomes narrower (Krag et al., 2014; Cuende et al., 2020) and fish are not able to fully utilize the meshes to escape (Fig. 5).

In *step 5*, we explored the effect of different θs on the size selection of Muller's pearlside and glacier lanternfish in trawls. For each *MS* and *OA* considered, we calculated the projected mesh size (*ms*) and projected mesh opening angle (*oa*) for different θ (Fig. 5), using equations 6–11. The angles considered ranged from 5° to 90°, in increments of 5°.

$$\frac{MW}{2} = \frac{MS}{2} \times \sin\frac{OA}{2} \tag{6}$$

$$\frac{ML}{2} = \frac{MS}{2} \times \cos\frac{OA}{2} \tag{7}$$

$$\frac{ml}{2} = \frac{MW}{2} \times \sin\theta \tag{8}$$

$$\frac{mw}{2} = \frac{MW}{2} \tag{9}$$

$$\frac{oa}{2} = \arctan\frac{\frac{ml}{2}}{\frac{MV}{2}} \tag{10}$$

$$ms = \sqrt{ml^2 + mw^2} \tag{11}$$

For the most relevant *MSs* used in the trawls described in section 2.1 (12, 20, 30, and 40 mm) and *OA*s ranging from 5° to 90°, the predicted *l50* values were summarized in isoline graphs (design guides). The dataset resulting from the above procedure was processed using the statistical software tool R (version 4.0.0; R Core Team (2020)). All plots were produced using the ggplot2 package (Wickham, 2016).

Finally, in *step 6*, we investigated whether the size selection obtained during experimental fishing could be understood based on the modelled simulation. The length frequency distributions of Muller's pearlsides collected by the 64-m long pelagic trawler "MS Ligrunn" with Trawl 3 were used. The catch data is based on 57 hauls carried out between June 19th and September 7th, 2019. The fishing grounds were off the west coast of Norway (58°02,00′ N - 61°34,00′ N, 01°42,00′ E – 05°24,00′ E). The total catch was 1223 tons of Muller's pearlside and the mean catch rate was 3.59 tons h^{-1}. Since the experimental fishery targeted the layer of Muller's pearlside between 180 and 200 m, glacier lanternfish, which normally is distributed below 400 m, was absent from the catches. in the catches. Underwater video was recorded using GoPro Hero4 Black edition cameras and red/infrared (620–630 nm) lights at some sampling stations to study fish behaviour relative to the trawl, small-meshed sections, and codend. These devices were attached inside and outside the trawl's top panel and at different locations along the trawl body, extension piece, and codend.

3. Results

3.1. Trawl parameters under operation

When operational, Trawl 1 had a vertical opening (height) of 64 m and a horizontal opening (width) of 90 m. At the start of the belly section with 8-m diamond meshes, these openings decreased to 56 and 80 m, respectively, resulting in a belly circumference of approximately 217 m and an estimated cross section of 3519 m^2. At the start of the 40-mm small-mesh liner, the height and width of the trawl was 32.5 m and 50 m, respectively, with a cross-section area of 1301 m^2. This gradually decreased to 18.1 m^2 in front of the codend causing large θs along the belly. The *OA*s in the belly varied between 40 and 46° (Fig. 6, Table 1). Trawl 2 had a height of 60 m and a width of 66 m. At the start of the belly section with the first 20-mm small-meshed liner, the height and width of the trawl was 48 and 48 m, respectively, with a cross-section area of 1809 m^2. This gradually decreased to 18.1 m^2 in front of the codend

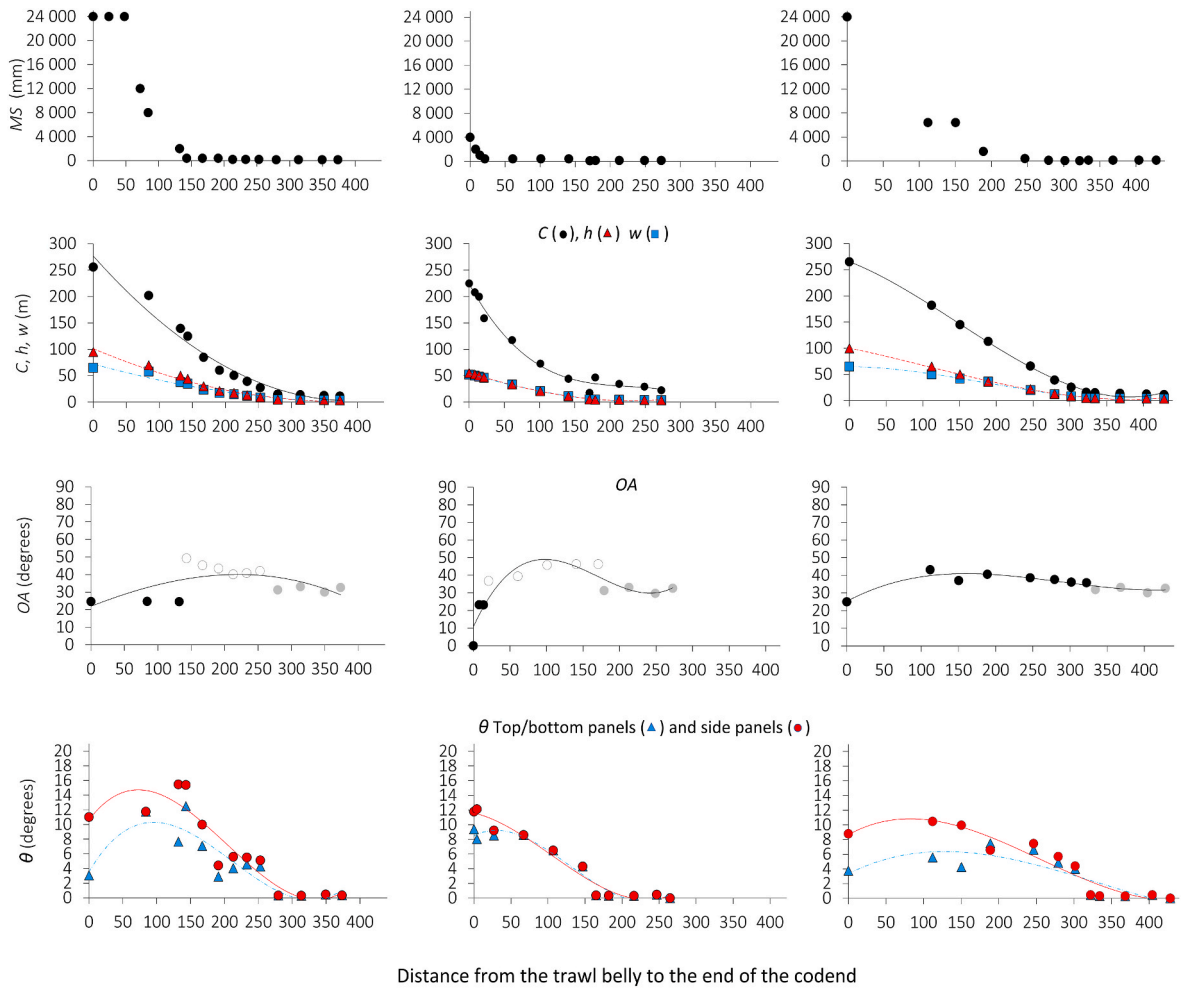

Fig. 6. Main design features of the trawls when operational. Trawl 1 (left column), Trawl 2 (centre column) and Trawl 3 (right column). The first row of figures shows the mesh sizes of the outer net and small-mesh liners along the trawl belly, extension piece, and codend. The second row shows the trawl circumference, height, and width of the trawls. The third row shows the opening angles for large meshes (black circles), small-mesh liners (white circles) and codend (grey circles) The fourth row shows the tapering angle of the top/bottom and side panels.

Table 1
Polynomial regressions describing the design features of the mesopelagic trawls. The trawl circumference (C), height (h), width (w), mesh opening angle (OA), and tapering angle (θ) are given as a function of the distance (x) from the belly to the end of the codend.

Parameter	Trawl 1		Trawl 2		Trawl 3	
	Polynomial regression fit	r^2	Polynomial regression fit	r^2	Polynomial regression fit	r^2
C	$9E\text{-}06x^3 - 0.003x^2 - 1.673x + 260.9$	0.987	$4E\text{–}0.6x^3 + 0.0012x^2 - 1.2064x + 170.3$	0.998	$6E\text{–}06x^3 - 0.0025x^2 - 0.5467x + 265.3$	0.998
h	$3E\text{-}06x^3 - 0.01x^2 - 0.303x + 96.4$	0.991	$9E\text{–}07x^3 + 0.0006x^2 - 0.416x + 55.6$	0.998	$2E\text{–}06x^3 - 0.0005x^2 - 0.295x + 100.4$	0.998
w	$3E\text{-}06x^3 - 0.001x^2 - 0.09x + 67.0$	0.979	$2E\text{–}06x^3 - 0.0002x^2 - 0.3511x + 52.8$	0.997	$2E\text{–}06x^3 - 0.0012x^2 + 0.0162x + 64.9$	0.996
OA	$-3E\text{–}07x^3 + 0.0002x^2 - 0.149x + 21.9$	0.417	$8E\text{–}06x^3 + 0.0041x^2 + 0.5889x + 20.3$	0.793	$1E\text{–}06x^3 - 0.001x^2 - 0.2246x + 25.2$	0.861
$\theta_{\text{top/bottom panels}}$	$2E\text{–}06x^3 + 0.001x^2 - 0.121x + 10.6$	0.871	$2E\text{–}0.6x^3 - 0.001x^2 + 0.0111x + 10.4$	0.951	$5E\text{–}07x^3 - 0.0004x^2 + 0.0561x + 5.6$	0.914
$\theta_{\text{side panels}}$	$2E\text{–}0.6x^3 - 0.001x^2 - 0.157x + 3.5$	0.819	$3E\text{–}06x^3 - 0.001x^2 + 0.0642x + 7.8$	0.962	$3E\text{–}07x^3 - 0.0002x^2 + 0.0513x + 3.3$	0.737

causing large θs along the belly. The resulting θs in the belly varied between 38 and 48° (Fig. 6, Table 1). Trawl 3 had a vertical opening (height) of 68 m and a horizontal opening of 96 m. At the start of the section with 3.2-m diamond meshes, these openings decreased to 46 and 57 m, respectively, resulting in a belly circumference of approximately 163 m and an estimated cross section area of 2059 m^2. This gradually decreased to 19.6 m^2 in front of the codend causing large θs along the belly. The resulting OAs in the belly varied between 35 and 40° (Fig. 6, Table 1).

3.2. Predicting the effect of mesh size, mesh opening angle, and tapering angle on size selectivity of Muller's pearlside and glacier lanternfish

A total of 311 Muller's pearlsides and 71 glacier lanternfish were used in the fall-through experiments to obtain a fall-through dataset for each of the 54 different mesh templates (Fig. 7). This resulted in 16794 and 3834 data points for Muller's pearlside and glacier lanternfish, respectively. The logit size selection (1) fitted to each of the fall-through datasets provided the $l50$ and SR for each mesh template (Figs. A1–A2 in the Appendix), which were subsequently used to establish a predictive model for size selection of Muller's pearlside and glacier lanternfish in trawls. From a total of 256 models tested for each species, the following

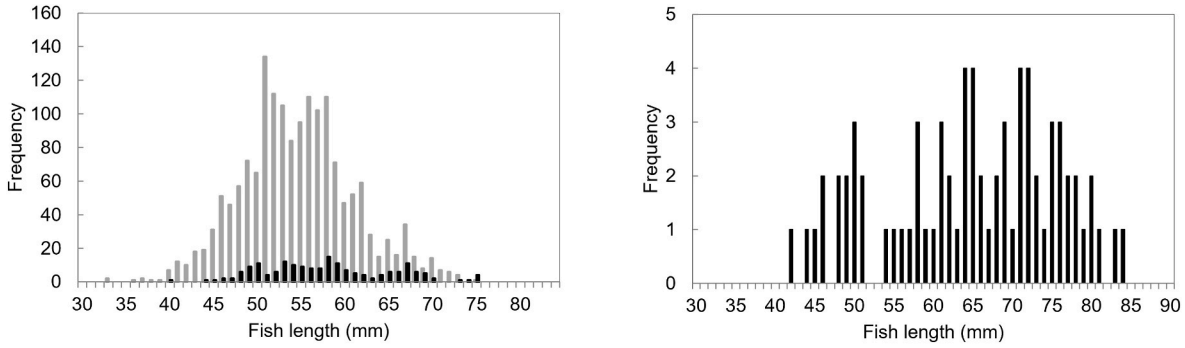

Fig. 7. Length frequency distribution of fish caught in the experimental fishery (grey bars) and fish used in the fall-through analysis (black bars).

model yielded smallest AICc value (referred to as the best model later in the text) for both species:

$$l50 = \alpha_1 \times ms \times oa + \alpha_2 \times ms \times oa^2 + \alpha_3 \times ms \times oa^3 \quad (12)$$

$$SR = \beta_1 \times ms \times oa + \beta_2 \times ms \times oa^2 \quad (13)$$

The model predictions plotted together with their respective 95% confidence intervals against the *l50* and *SR* values estimated by fitting a logit size selection model Eq. (3) to each fall-through dataset reveal that the models represent the trends in the fall through data well for both species (Figs. A3–A10 in the Appendix). Therefore, the model can be used to predict size selection of Muller's pearlside and glacier lanternfish in trawls for the range of *MS* and *OA*. The model coefficients obtained for each species are presented in Table 2.

Using the best predictive model (12), the following design guides (Fig. 8A – B) were created depicting the effect of *MS* and *OA* on size selection of optimally oriented Muller's pearlside and glacier lanternfish when encountering trawl meshes. From both figures, it can be seen that a decrease in *OA* from 90° to ~40° has a negligible effect on the *L50* values for both species. Further decreases in *OA* results in lower *l50* values. The increase in *MS* from 5 to ~30 mm results in a larger increase in *l50* values, compared to the same increase in *MS* in the ~30–60 mm range.

Figs. 9 and 10 illustrate how *l50* values vary with the change in *OA* and θ for selected *MS*s for Muller's pearlside and glacier lanternfish, respectively. From both figures it is evident that lower *MS*s (12 mm and 16 mm) are more suitable options for catching both species.

3.3. Experimental fishing with Trawl 3

Muller's pearlsides displayed active trawl avoidance and escape behaviour through the trawl panels in the belly of Trawl 3. Trawl avoidance was monitored by observing the ecograms of the hull mounted echosounder and those of the trawl sonar. Muller's pearlsides either dive and avoid the incoming trawl or are concentrated in the middle of the trawl's path. Muller's pearlsides entering the trawl actively avoided the net panels in front of the trawl. As they were herded and concentrated inside the trawl, fish started displaying active escape behaviour. Large numbers of Muller's pearlsides were observed escaping through the 30 mm meshes in the extension piece of Trawl 3 (Fig. 11). Water flow in the joint between the trawl's extension piece and codend was 1.1 ± 0.1 ms^{-1}. Despite large losses of fish in the belly and extension piece, Trawl 3 yielded mean catch rates of 3.59 tons h^{-1}. The size frequency distribution of Muller's pearlside caught by Trawl 3 showed that most fish were between 40 and 70 mm, with largest modes between 50 and 60 mm.

Table 2
Results for fitting the best model (12) to the fall-through size selectivity data for Muller's pearlside and glacier lanternfish. Values in brackets represent 95% confidence intervals.

Species	Parameter	Factor	Value	P-value
Pearlside	*l50* (mm)	α_1	1.35E-0.1 (1.26E-01 – 1.43E-0.1)	<0.0001
		α_2	−1.56E-03 (−1.56E-03 + 1.26E-03)	<0.0001
		α_3	5.73E-06 (3.31E-06 – 8.16E-06)	<0.0001
	SR (mm)	β_1	5.41E-03 (4.41E-03 – 6.42E-03)	<0.0001
		β_2	−4.09E-05 (−5.58E-05 + 2.60E-05)	<0.0001
Lanternfish	*l50* (mm)	α_1	1.02E-02 (9.51E-03 – 1.10E-02)	<0.0001
		α_2	−1.07E-07 (−1.31E-04 + 8.29E-05)	<0.0001
		α_3	3.70E-07 (1.80E-07 – 5.60E-07)	<0.0001
	SR (mm)	β_1	1.04E-03 (7.10E-04 – 1.36E-03)	<0.0001
		β_2	−8.71E-06 (−1.33E-05 + 4.17E-06)	<0.0001

4. Discussion

Two major factors that determine the catch efficiency of complex mesopelagic trawls are fish avoidance of the incoming trawl and mesh selection along the entire trawl (trawl belly, extension piece, and codend). Both factors are strongly dependent on the fish species, (i.e., their size, shape, swimming ability, endurance), trawl design features (i.e., trawls with different mesh sizes, opening angles, and tapering angles), and operational conditions (i.e., tow speed).

Avoidance behaviour from mesopelagic trawls towed at 2–3 knots has been reported in many studies (Gjøsæter and Kawaguchi, 1980; Kaartvedt et al., 2012; Davison et al., 2015; Underwood et al., 2020) as one of the main reasons why trawl-based estimates of mesopelagic fish biomass are underestimated and considerably lower than acoustic-based estimates. Consequently, trawl avoidance may be an issue for Trawl 1 and Trawl 2 because these trawls (with a total drag larger than 42 tons) are limited to being towed at low speeds (2.2–2.4 knots). Fish avoidance from these trawls can potentially be reduced by increasing the towing speed. However, this will increase the total drag considerably, and thus the energy power necessary to tow the trawls. Trawl 3, which is lighter than Trawl 1 and Trawl 2, due to the absence of small-mesh liners, can be towed faster and potentially reduce fish avoidance.

Fish that enter the trawls are exposed to mesh selectivity along the entire trawl body. Therefore, the trawls with small-mesh lines may be better at reducing unwanted size selection along the trawl's belly and extension piece. Generally, the density of fish that enters the trawl increases as it moves towards the codend because the fish get concentrated by the low tapered liners. Therefore, a gradual decrease in mesh size in the liners can potentially enhance size selectivity before these species enter the codend. Active escape behaviour of Muller's pearlsides, and passive filtering of glacier lanternfish have been observed in the belly of mesopelagic trawls analysed in this study at tow speeds of 2.2–2.4 knots (Grimaldo et al., 2020; Bjordal and Thorvaldsen, 2020).

Therefore, identifying the areas with high escape rates in the trawl

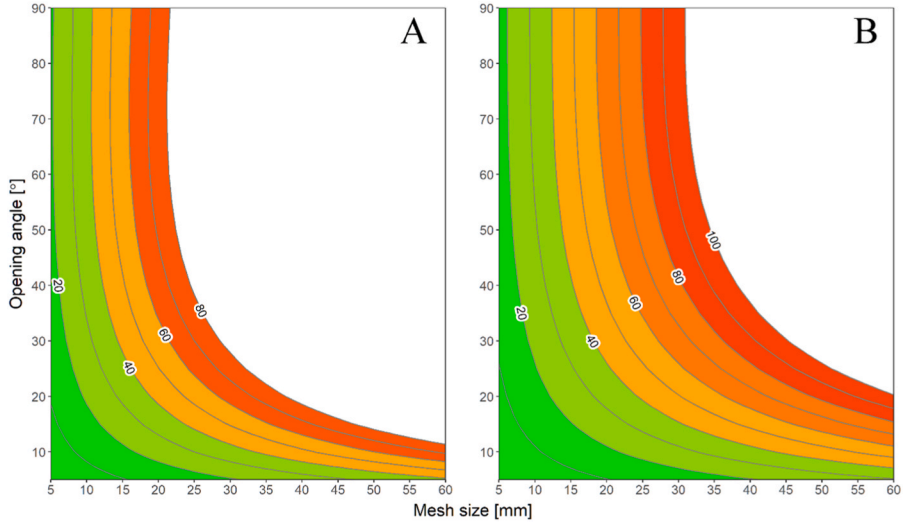

Fig. 8. Design guides showing the effect of mesh size (*MS*) and opening angle (*OA*) on *l50* values for optimally oriented Muller's pearlside (A) and glacier lanternfish (B). Muller's pearlside and glacier lanternfish grow up to 8 and 10 cm, respectively. The more pronounced red colour on the plot indicates greater catch loss of the species. (For interpretation of the references to colour in this figure legend, the reader is referred to the Web version of this article.)

and optimizing size selectivity could reduce unwanted loss of fish in the trawl belly and help to improve catch rates, making the fishery more cost efficient. This study applied a model to predict the effect of trawl design features on two common mesopelagic species (Muller's pearlside and glacier lanternfish) experimentally caught in the Northeast Atlantic and Norwegian EEZ. Instead of building a model that was based on expensive and time-limited sea trials assessing the selectivity of large and complex trawl structures, our model was constructed with data based on fall through experiments that were carried out in the laboratory using samples collected in commercial trials. This kind of modelling to assess size selectivity has previously been successfully applied to investigating size selection of Nephrops *Nephrops norvegicus* in the Adriatic pot fishery (Brčić et al., 2018) and snow crab in the Barents Sea (Herrmann et al. 2021). In this study, we show that the same methods can also be applied to the assess the selectivity of complex mesopelagic trawl systems, and that our model can be used to predict the potential catch loss though meshes along the entire trawl. We used the model to further investigate the effect of mesh size, tapering angle, and mesh opening on the size selectivity of three trawls that have been used by pelagic trawlers targeting mesopelagic species in the Northeast Atlantic Ocean and the Norwegian EEZ. Our prediction model is supplemented by length frequency distributions of Muller's pearlsides obtained from an experimental fishery using one of the trawls analysed in this study.

Our model predicts that most fish smaller than 40 mm can be released by the 20 mm liners with mesh opening angles of 30–40° which equal those measured in the extension piece of Trawl 1 and Trawl 2. Likewise, our model predicts that small-mesh liners of 40, 30, and 20 mm, as used in the belly of Trawl 1, allow for a considerable proportion of Muller's pearlside and glacier lanternfish to be sorted out in the trawl belly. Moreover, under the assumption of no fish herding by the 40- and 30-mm liners, the liners only increase the total drag of the trawl and limit the speed at which the trawl can be towed. In addition, when entering the codend, a large number of small individuals may also escape as a result of stacking and squeezing. However, since Trawl 3 does not have small-mesh liners in the belly or extension piece, active fish selection can happen along the entire trawl body. Underwater video recordings and enmeshing of fish in the 30 mm meshes of Trawl 3 support this. Consequently, under the assumption that no fish herding is caused by the meshes in the trawl belly, our model suggests that Trawl 3 is the least effective of the three trawls analysed in this study. Trawl 2, with 20 mm liners along the entire belly and extension piece, is the best trawl design in terms of limiting the loss of fish in these parts of the trawl according to our model. Despite our model suggesting that the meshes of the 20 mm liners, with 30°–50° mesh opening angles at 2°–12° tapering angles (angle of attack), may lose up to 30% Muller's pearlside and glacier lanternfish (Fig. 8) along the belly and extension piece, Trawl 2 with its large effective cross-section area (1809 m^2), is still the trawl with largest predicted catch efficiency. Despite large loses of fish in the belly and extension piece, Trawl 3 yielded mean catch rates of 3.59 tons h^{-1}. Based on our prediction models (Fig. 9), catches could have been 2–3 times larger (up to 10 tons h^{-1}) if the pelagic trawler MS Ligrunn had used Trawl 2 instead of Trawl 3.

In conclusion, our prediction models suggest that Trawl 2 may be the best trawl design for reducing the loss of mesopelagic fish (Muller's pearlside and glacier lanternfish) caused by mesh selection along the belly and extension piece. Despite Trawl 2 having a potential risk of losing 30% of fish through mesh selection along the belly, the effective fishing area of this trawl is large enough (1809 m^2) to still yield large catches of mesopelagic fish. Further improvements to this trawl can be achieved by reducing the effective cross section area (area at which the first 20 mm small-mesh liner is attached to the trawl belly) to reduce the total drag and facilitate an increased towing speed (i.e., from 2.2 to 2.4 to 3.5 knots for instance) to reduce fish avoidance. Actual field measurements of tow speed, trawl drag, and water flow, as well as underwater video observations to monitor fish behaviour are needed to verify this hypothesis.

Data availability statement

The original contributions presented in the study are included in the article/Supplementary Material. Further inquiries can be directed to the corresponding author/s.

CRediT authorship contribution statement

Eduardo Grimaldo: Conceptualization, Data curation, Writing – original draft, Writing – review & editing. **Bent Herrmann:** Conceptualization, Validation, Writing – original draft, Writing – review & editing. **Jure Brčić:** Conceptualization, Validation, Writing – original draft, Writing – review & editing. **Kristine Cerbule:** Data curation, Validation, Writing – original draft. **Jesse Brinkhof:** Writing – original draft. **Leif Grimsmo:** Investigation, Data curation. **Nadine Jacques:** Data curation.

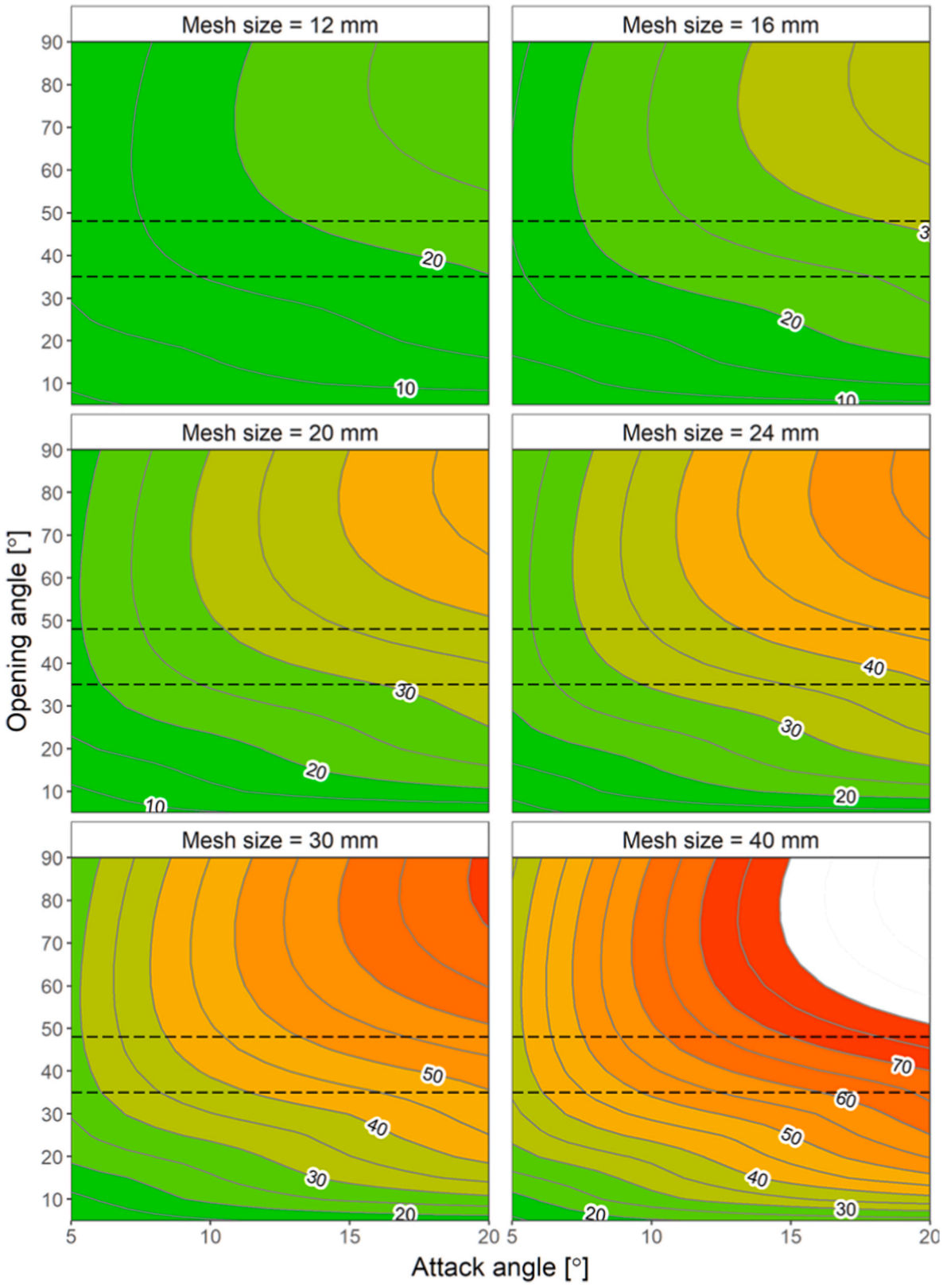

Fig. 9. Predicted *l50* values for Muller's pearlside (in mm) for different tapering angles (θ) and mesh opening angles (*OA*) for selected mesh sizes (*MS*) (12 mm, 16 mm, 20 mm, 24 mm, 30 mm, and 40 mm). Muller's pearlside grow up to 8 cm and the more pronounced red colour on the plot indicates greater catch loss of the species. (For interpretation of the references to colour in this figure legend, the reader is referred to the Web version of this article.)

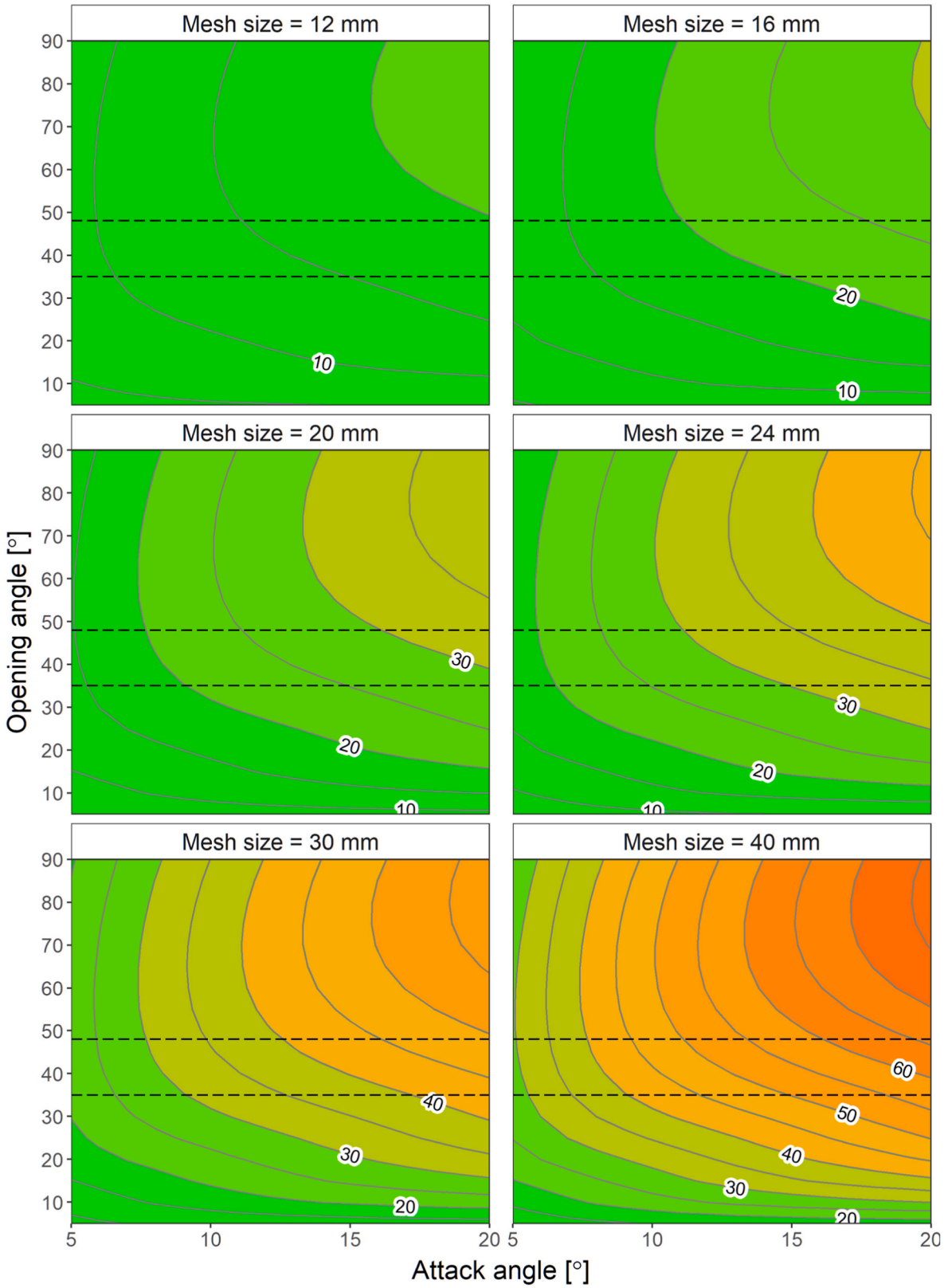

Fig. 10. Predicted *l50* values for glacier lanternfish (in mm) for different tapering angles (θ) and mesh opening angles (*OA*) for selected mesh sizes (12 mm, 16 mm, 20 mm, 24 mm, 30 mm, and 40 mm). Glacier lanternfish grow up to 8 cm and the more pronounced red colour on the plot indicates greater catch loss of the species. (For interpretation of the references to colour in this figure legend, the reader is referred to the Web version of this article.)

Fig. 11. Image inside (left) and outside (right) of the trawl's extension showing active escape behaviour of Muller's pearlsides through the 30 mm meshes of the extension piece of Trawl 3.

Declaration of competing interest

The authors declare that they have no known competing financial interests or personal relationships that could have appeared to influence the work reported in this paper.

Acknowledgments

We thank the company Br. Birkeland Fiskebåtrederi AS for providing the trawl drawings that were analysed in this study. This work was supported by the EU H2020 project MEESO, grant number 817669.

Appendix A. Supplementary data

Supplementary data to this article can be found online at https://doi.org/10.1016/j.oceaneng.2022.111964.

Appendix A

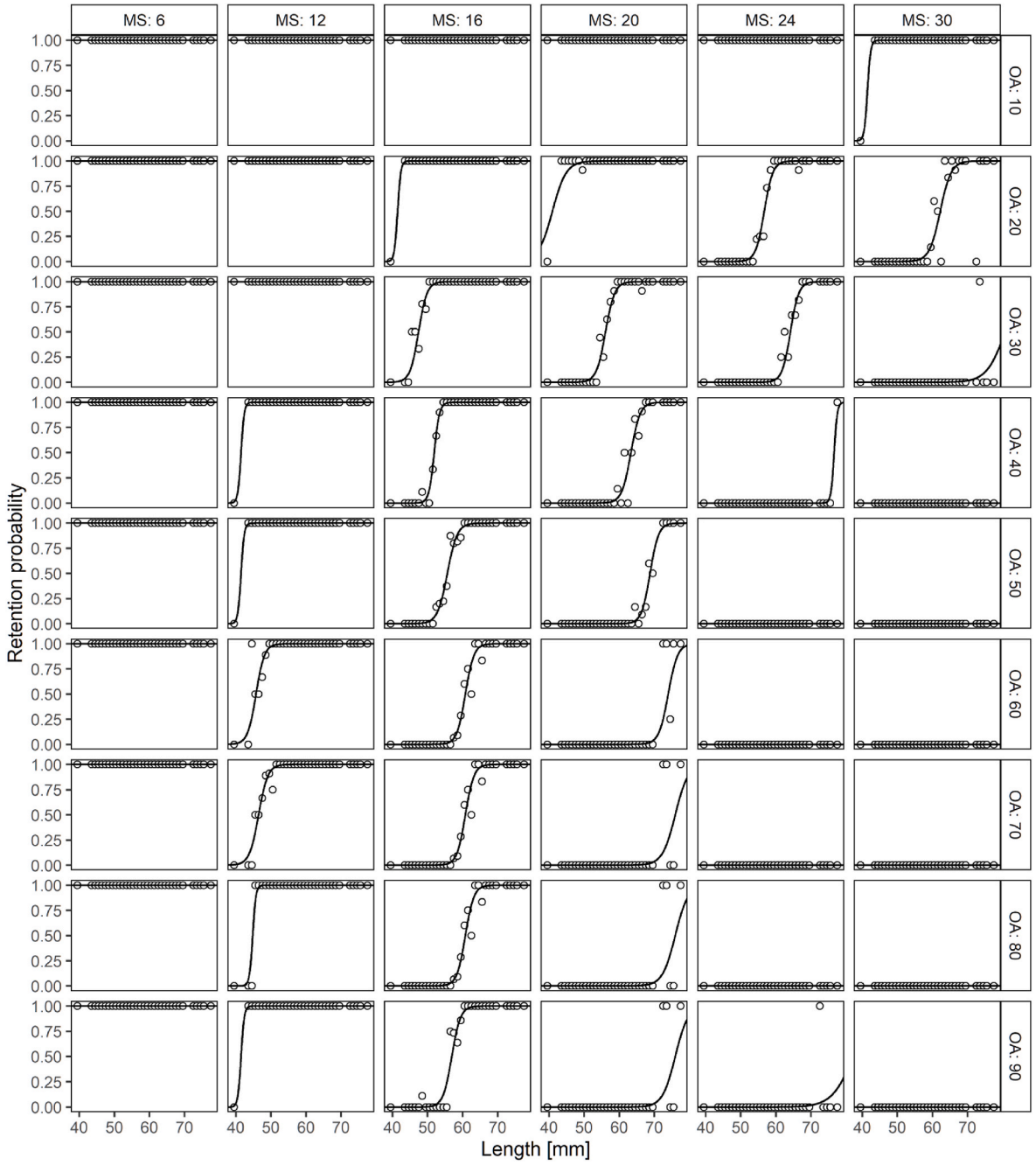

Fig. A1. The fall-through size selection curves for each mesh template for Muller's pearlside. The fall-through rates are represented by black circles and the fitted logit size selection models are represented by lines. MS: mesh size in mm; OA: opening angle in degrees.

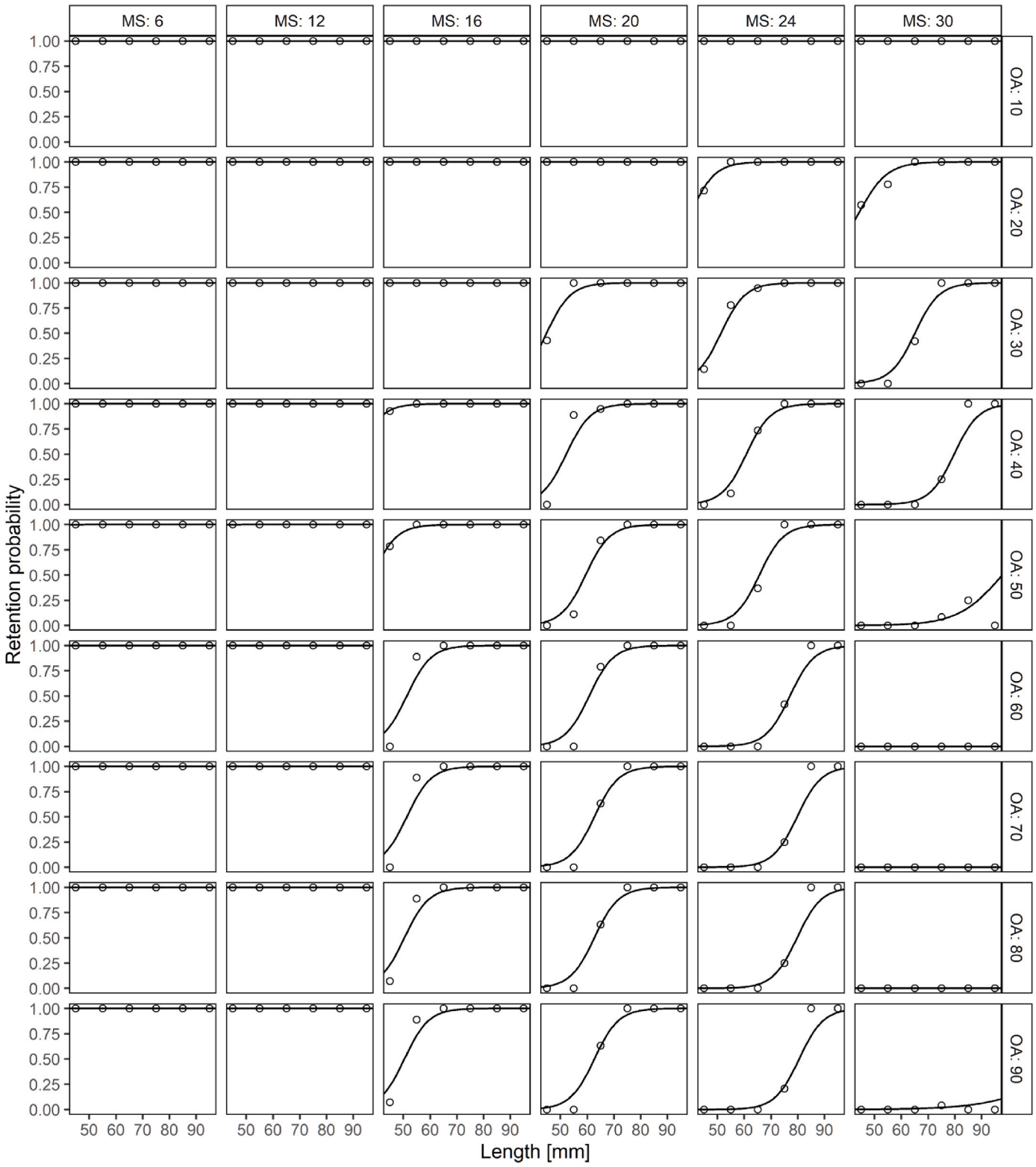

Fig. A2. The fall-through size selection curves for each mesh template for glacier lanternfish. The fall-through rates are represented by black circles and the fitted logit size selection models are represented by lines. MS: mesh size in mm; OA: opening angle in degrees.

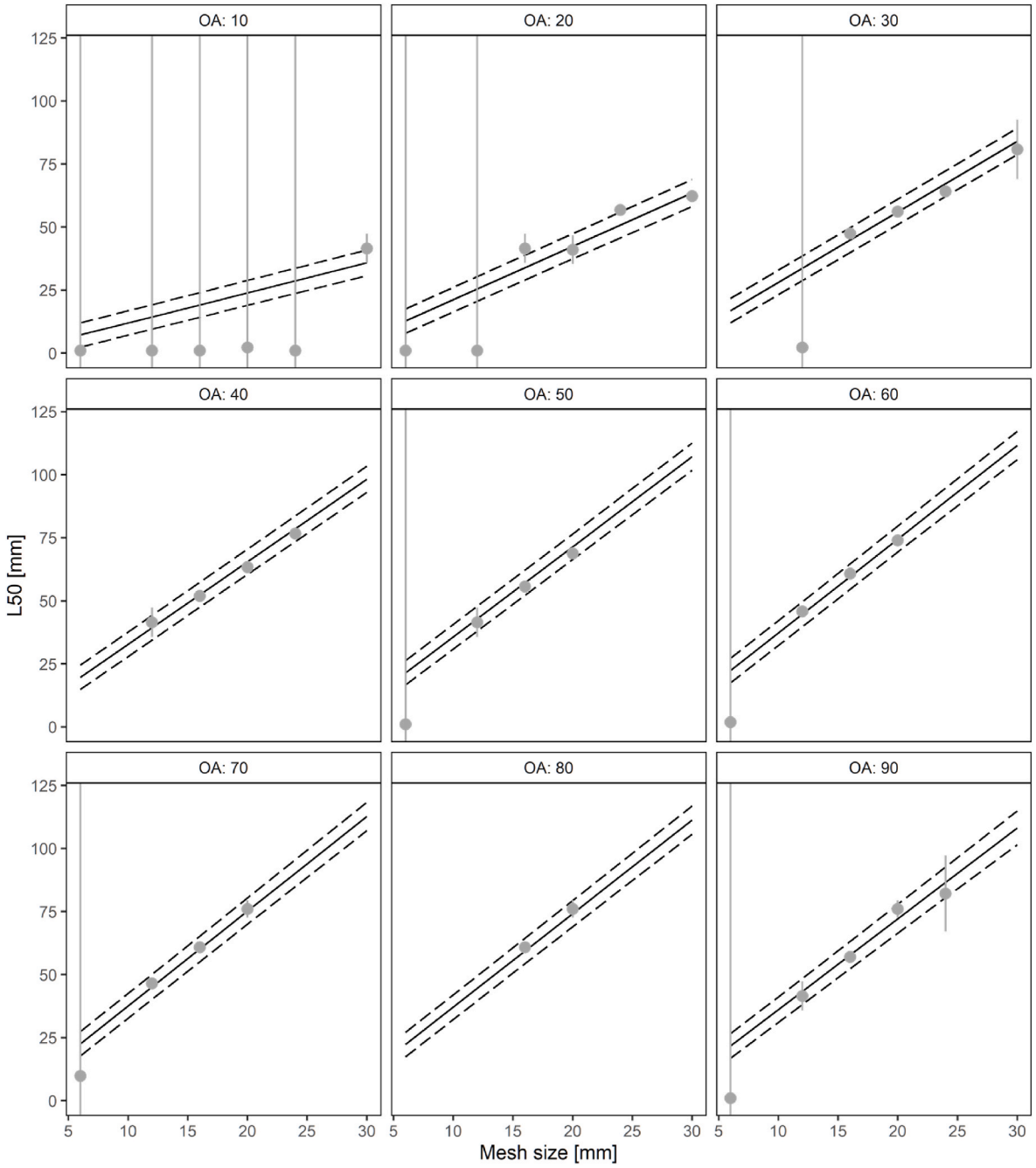

Fig. A3. Predicted L50 values using Eq. (11) versus mesh size for each mesh opening angle used in the fall-through experiments for Muller's pearlside. The solid lines represent predicted mean values and dashed lines represent 95% confidence intervals. Grey points represent L50 estimates with their respective 95% confidence intervals for each fall-through size selection curve.

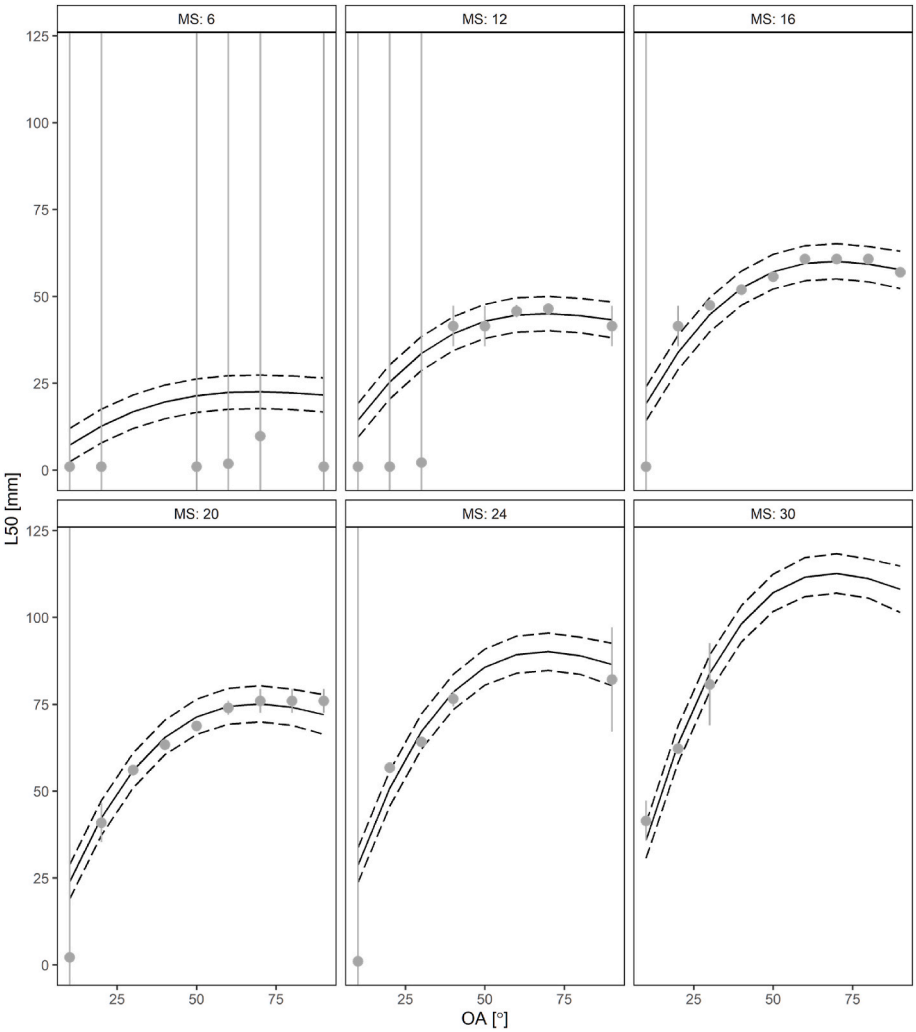

Fig. A4. Predicted L50 values using Eq. (11) versus opening angle for each mesh size used in the fall-through experiments for Muller's pearlside. The solid lines represent predicted mean values and dashed lines represent 95% confidence intervals. Grey points represent L50 estimates with their respective 95% confidence intervals for each fall-through size selection curve.

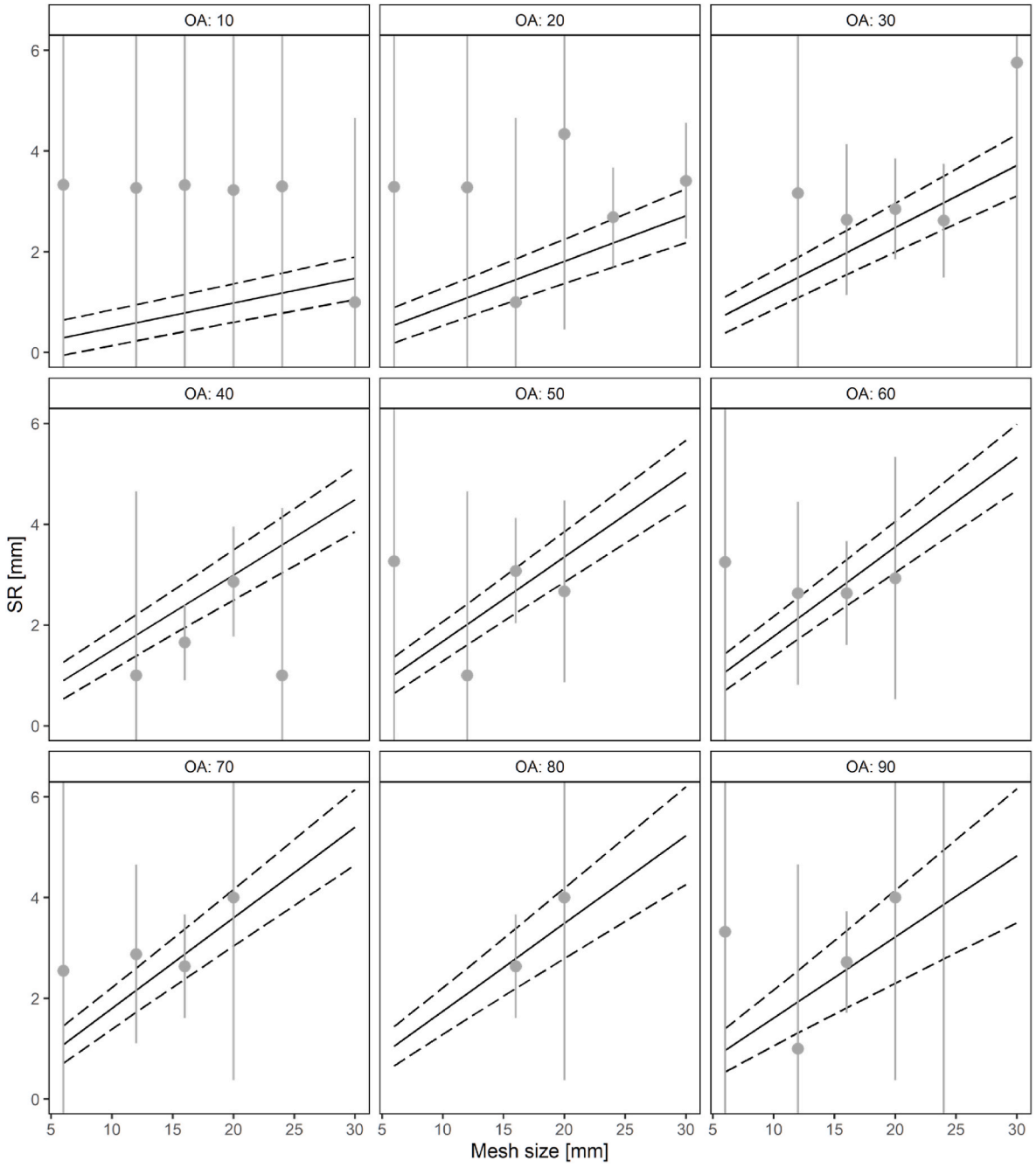

Fig. A5. Predicted SR values using Eq. (11) versus mesh size for each mesh opening angle used in the fall-through experiments for Muller's pearlside. The solid lines represent predicted mean values and dashed lines represent 95% confidence intervals. Grey points represent SR estimates with their respective 95% confidence intervals for each fall-through size selection curve.

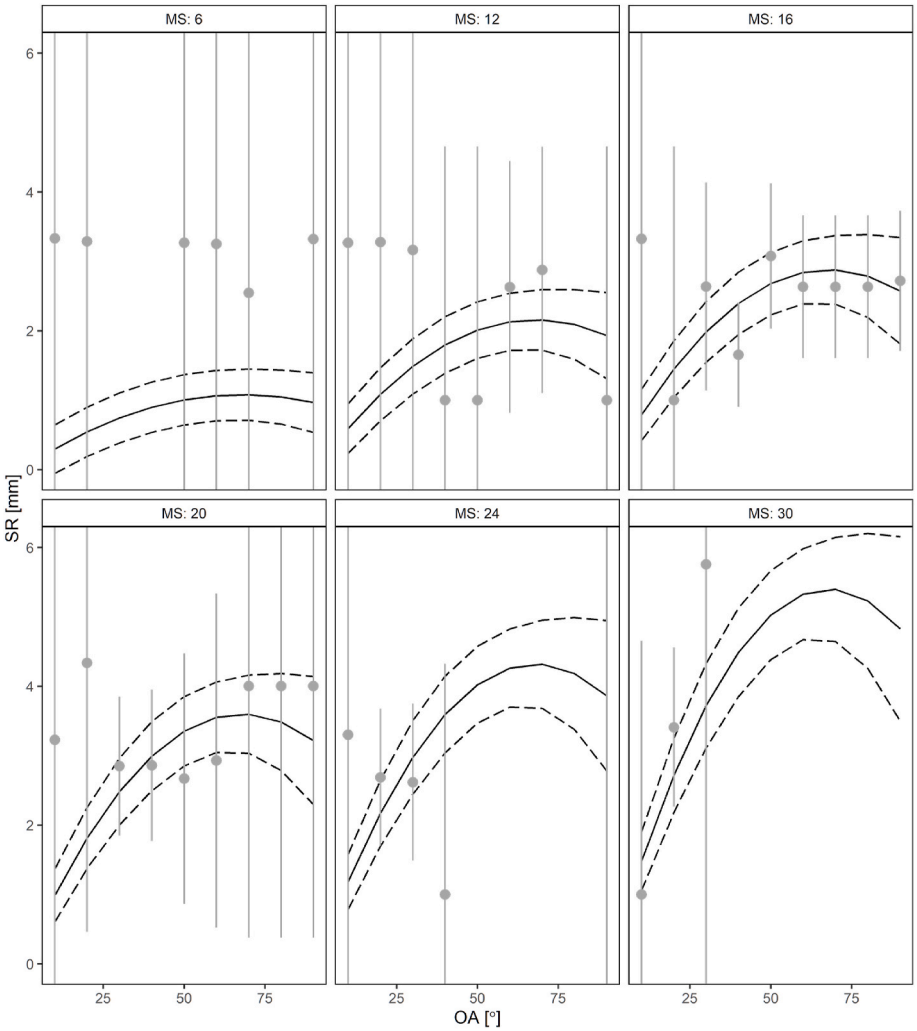

Fig. A6. Predicted SR values using Eq. (11) versus mesh opening angle for each mesh size used in the fall-through experiments for Muller's pearlside. The solid lines represent predicted mean values and dashed lines represent 95% confidence intervals. Grey points represent SR estimates with their respective 95% confidence intervals for each fall-through size selection curve.

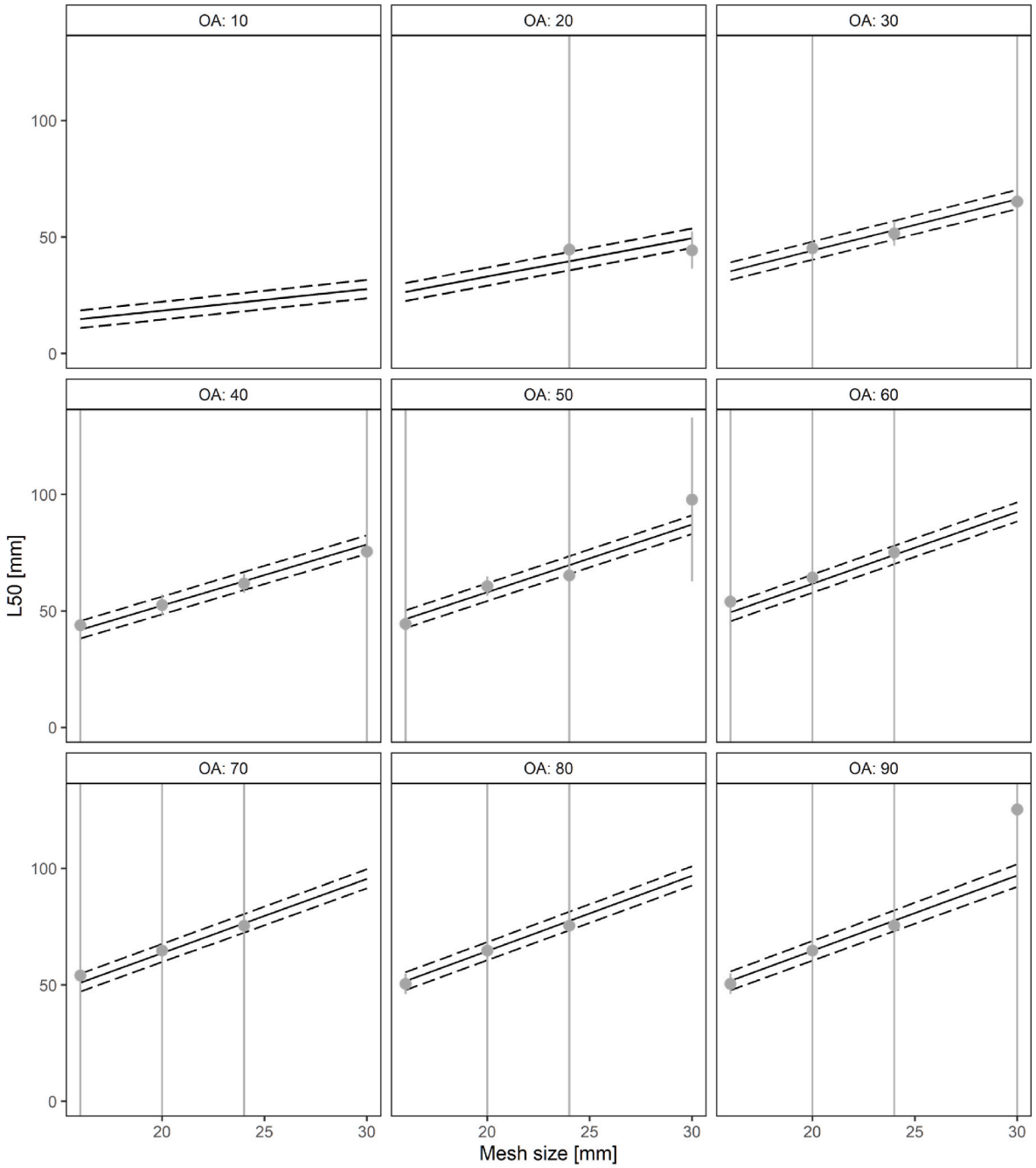

Fig. A7. Predicted L50 values using Eq. (11) versus mesh size for each mesh opening angle used in the fall-through experiments for glacier lanternfish. The solid lines represent predicted mean values and dashed lines represent 95% confidence intervals. Grey points represent L50 estimates with their respective 95% confidence intervals for each fall-through size selection curve.

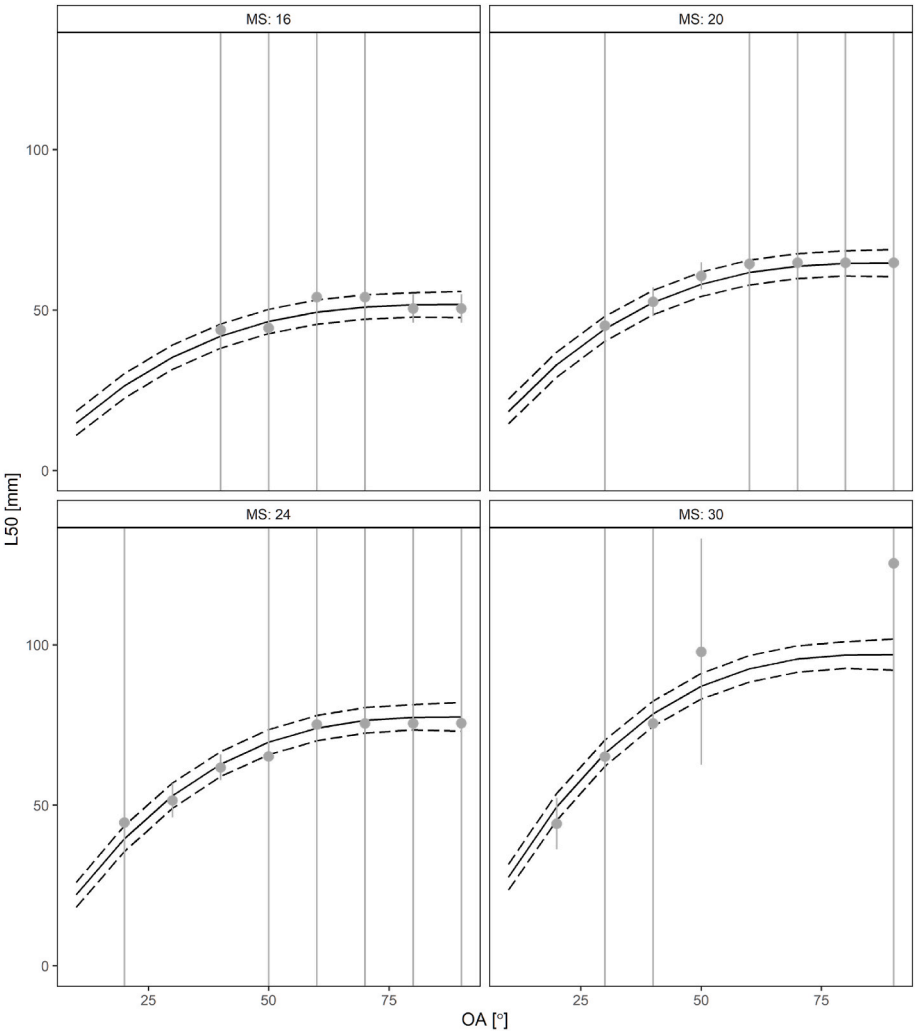

Fig. A8. Predicted L50 values using Eq. (11) versus opening angle for each mesh size used in the fall-through experiments for glacier lanternfish. The solid lines represent predicted mean values and dashed lines represent 95% confidence intervals. Grey points represent L50 estimates with their respective 95% confidence intervals for each fall-through size selection curve.

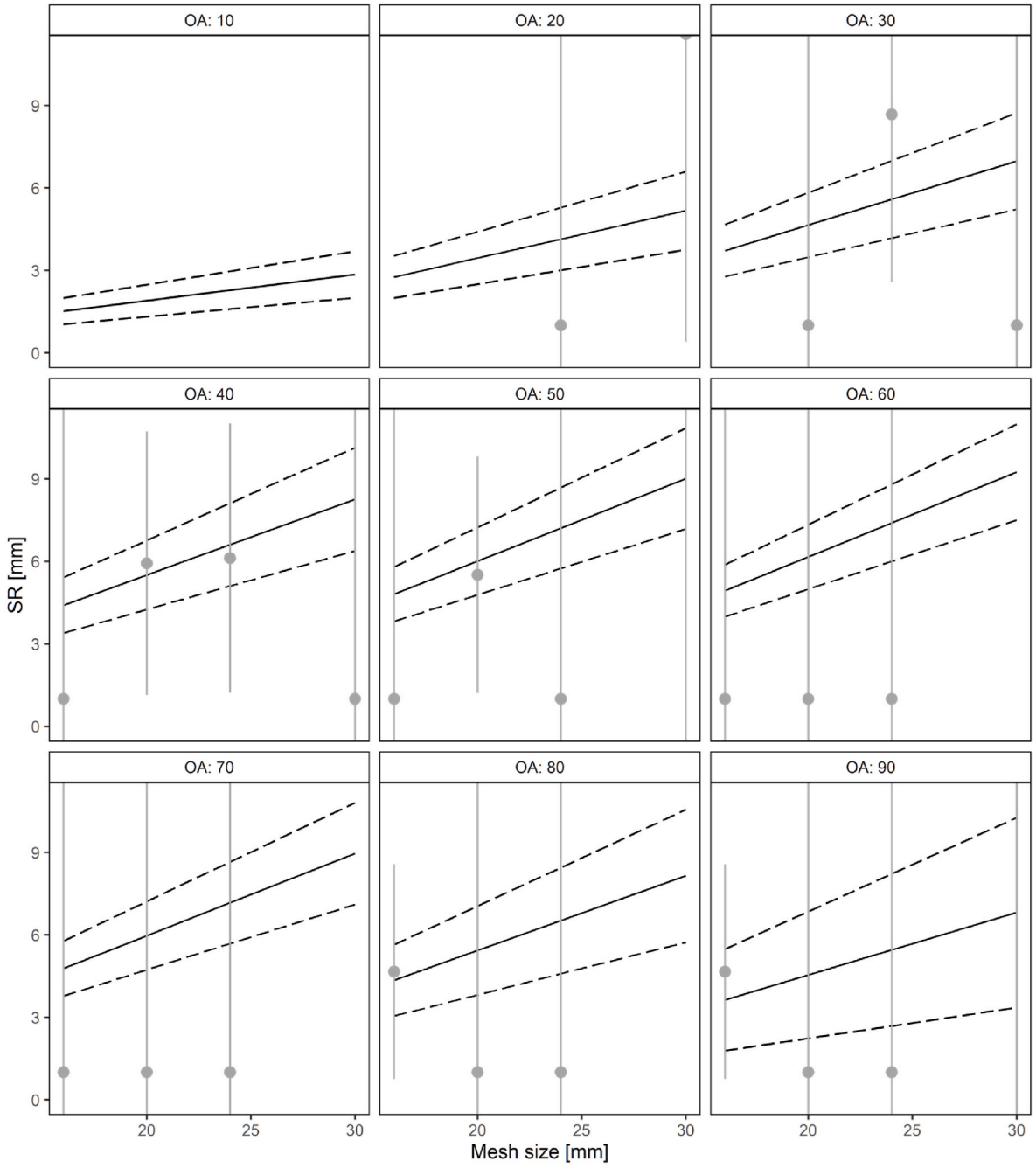

Fig. A9. Predicted SR values using Eq. (11) versus mesh size for each mesh opening angle used in the fall-through experiments for glacier lanternfish. The solid lines represent predicted mean values and dashed lines represent 95% confidence intervals. Grey points represent SR estimates with their respective 95% confidence intervals for each fall-through size selection curve.

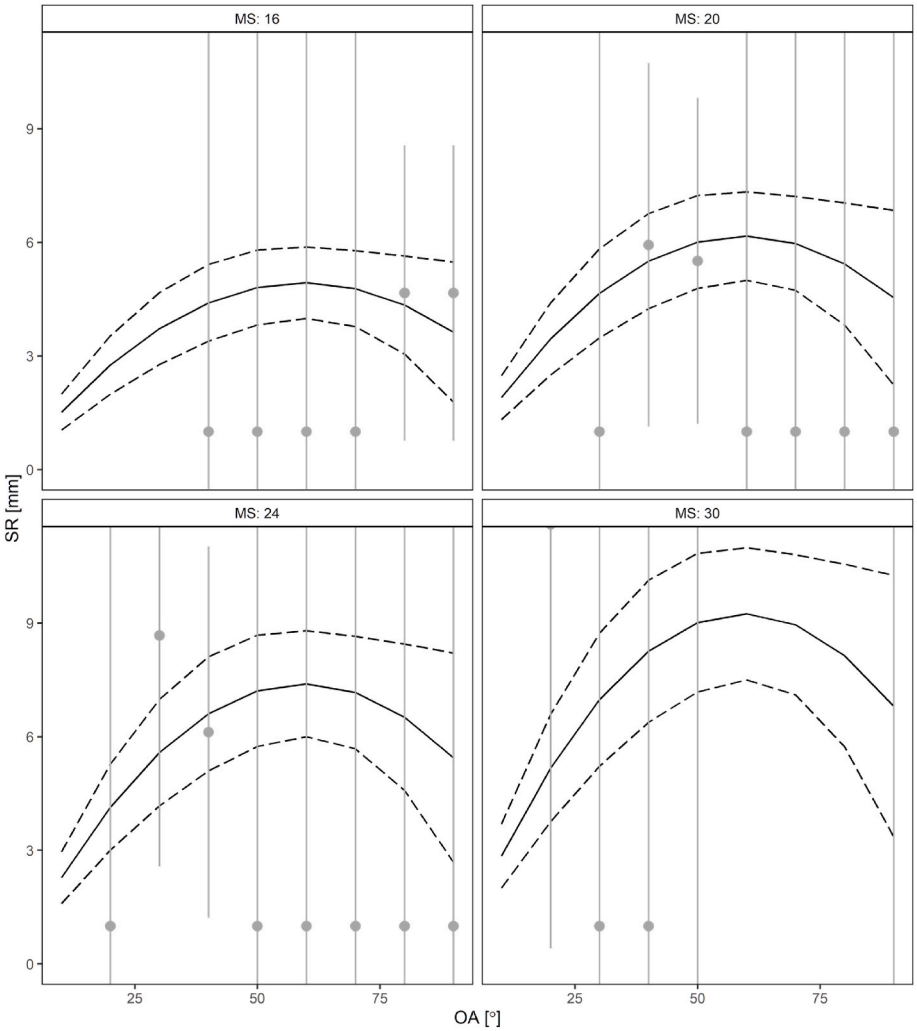

Fig. A10. Predicted SR values using Eq. (11) versus mesh opening angle for each mesh size used in the fall-through experiments for glacier lanternfish. The solid lines represent predicted mean values and dashed lines represent 95% confidence intervals. Grey points represent SR estimates with their respective 95% confidence intervals for each fall-through size selection curve.

References

Akaike, 1974. A new look at the statistical model identification. IEEE Trans. Autom. Control, AC 19, 716–723. https://doi.org/10.1109/TAC.1974.1100705.

Barkley, R.A., 1972. Selectivity of towed-net samplers. Fish. Bull. 70, 799–820.

Bjordal, Å., Thorvaldsen, K.G., 2020. Trial Fisheries for Mesopelagic Species 2019 - Summary. Report from the Institute of Marine Research. IMR) 2020-5, ISSN: 1893-4536. 2020. (In Norwegian).

Boyra, G., Martínez, U., Cotano, U., Santos, M., Irigoien, X., Uriarte, A., 2013. Acoustic surveys for juvenile anchovy in the Bay of Biscay: abundance estimate as an indicator of the next year's recruitment and spatial distribution patterns. ICES (Int. Counc. Explor. Sea) J. Mar. Sci. 70 (7), 1354–1368. https://doi.org/10.1093/icesjms/fst096.

Brčić, J., Herrmann, B., Mašanović, M., Šifner, S.K., Škeljo, F., 2018. CREELSELECT- A method for determining the optimal creel mesh: case study on Norway lobster (*Nephrops norvegicus*) fishery in the Mediterranean Sea. Fish. Res. 204, 433–440. https://doi.org/10.1016/j.fishres.2018.03.020.

Briggs, R., 1992. An assessment of nets with a square mesh panel as a whiting conservation tool in the Irish Sea Nephrops fishery. Fish. Res. 13, 133–152.

Briggs, R., Robertson, J., 1993. Square mesh panel studies in the Irish Sea Nephrops fishery. ICES C.M. 1993/B20 1–10.

Burnham, K.P., Anderson, D.R., 2002. Model Selection and Multimodel Inference: A Practical Information-Theoretic Approach, second ed. Springer, New York.

Cuende, E., Arregi, L., Herrmann, B., Sistiaga, M.B., Aboitiz, 2020. Prediction of square mesh panel and codend size selectivity of blue whiting based on fish morphology. ICES (Int. Counc. Explor. Sea) J. Mar. Sci. https://doi.org/10.1093/icesjms/fsaa156.

Davison, P.C., Koslow, J.A., Kloser, R.J., 2015. Acoustic biomass estimation of mesopelagic fish: backscattering from individuals, populations, and communities. ICES (Int. Counc. Explor. Sea) J. Mar. Sci. 72 (5), 1413–1424. https://doi.org/10.1093/icesjms/fsv023.

FAO, 1997. Review of the State of the World Fisheries Resources: Marine Fisheries. FAO Fisheries Circular No.920, Rome, Italy. 173pp. ISSN 0429-9329. http://www.fao.org/3/w4248e/w4248e00.htm.

Fridman, A.L., 1966. Calculations for fishing gear designs. FAO fishing manuals. FAO Fishing News.

Gjøsæter, J., Kawaguchi, K., 1980. A Review of the World Resources of Mesopelagic Fish. FAO Fisheries Technical Paper No. 193, 151pp.

Grimaldo, E., Grimsmo, L., Alvarez, P., Herrmann, B., Tveit, G.M., Tiller, R., Slizyte, R., Aldanondo, N., Guldberg, T., Toldnes, B., Carvajal, A., Schei, M., Selnes, M., 2020. Investigating the potential for a commercial fishery in the Northeast Atlantic utilizing mesopelagic species. ICES (Int. Counc. Explor. Sea) J. Mar. Sci. 77 (7–8), 2541–2556. https://doi.org/10.1093/icesjms/fsaa114.

Heino, M., Porteiro, F.M., Sutton, T.T., Falkenhaug, T., Godø, O.R., Piatkowski, U., 2011. Catchability of pelagic trawls for sampling deep-living nekton in the mid-North Atlantic. ICES (Int. Counc. Explor. Sea) J. Mar. Sci. 68 (2), 377–389. https://doi.org/10.1093/icesjms/fsq089.

Herrmann, B., Krag, L.A., Frandsen, R.P., Madsen, N., Sthr, K.J., 2009. Prediction of selectivity from morphological conditions: methodology and a case study on cod (*Gadus morhua*). Fish. Res. 97, 59–71. https://doi.org/10.1016/j.fishres.2009.01.002.

Herrmann, B., Sistiaga, M., Nielsen, K., Larsen, R.B., 2012. Understanding the size selectivity of redfish (*Sebastes spp.*) in North Atlantic trawl codends. J. Northwest Atl. Fish. Sci. 44, 1–13. https://doi.org/10.2960/J.v44.m680.

Herrmann, B., Krag, L.A., Krafft, B.A., 2018. Size selection of antarctic krill (*Euphausia superba*) in a commercial codend and trawl body. Fish. Res. 207, 49–54. https://doi.org/10.1371/journal.pone.0102168.

Hidalgo, M., Browman, H.I., 2019. Developing the knowledge base needed to sustainably manage mesopelagic resources. ICES (Int. Counc. Explor. Sea) J. Mar. Sci. 76 (3), 609–615. https://doi.org/10.1093/icesjms/fsz067.

Hulley, P.A., 1990. Myctophidae. P. 398-467. In: Quero, J.C., Hureau, J.C., Karrer, C., Post, A., Saldanha, L. (Eds.), Check-list of the Fishes of the Eastern Tropical Atlantic (CLOFETA). JNICT, Lisbon; SEI, vol. 1. Paris; and UNESCO, Paris.

Irigoien, X., Klevjer, T., Røstad, A., Martinez, U., Boyra, G., Acuña, J., Bode, F., et al., 2014. Large mesopelagic fishes biomass and trophic efficiency in the open ocean. Nat. Commun. 5 (1), 1–10. https://doi.org/10.1038/ncomms4271.

St John, M.A., Borja, A., Chust, G., Heath, M., Grigorov, L., Mariani, P., Martin, A.P., et al., 2016. A dark horse in our understanding of marine ecosystems and their services: perspectives from the mesopelagic community. Front. Mar. Sci. 3, 1–6. https://doi.org/10.3389/fmars.2016.00031.

Kaartvedt, S., Staby, A., Aksnes, D.L., 2012. Efficient trawl avoidance by mesopelagic fishes causes large underestimation of their biomass. Mar. Ecol. Prog. Ser. 456, 1–6. https://doi.org/10.3354/meps09785.

Krag, L.A., Herrmann, B., Iversen, S.A., Engås, A., Nordrum, S., Krafft, B.A., 2014. Size selection of antarctic krill (*Euphausia superba*) in trawls. PLoS One 9 (8), e102168. https://doi.org/10.1371/journal.pone.0102168, 2014.

Lee, K.-T., Lee, M.-A., Wang, J.-P., 1996. Behavioural responses of larval anchovy schools herded within large-mesh wings of trawl net. Fish. Res. 28, 57–69. https://doi.org/10.1016/0165-7836(96)00485-7.

Li, L.Z., Chen, S., Yang, J.L., Liu, J., Wu, Y., Qu, T.C., Rao, X., Huang, H.L., 2017. Performance analysis of the four-panel mid-water trawl for Antarctic krill fishery. J. Fish. Sci. China 24 (4), 893–901 (in Chinese with English abstract). http://www.aquaticjournal.com/article/doi/10.3724/SP.J.1118.2017.16288.

Muus, B.J., Nielsen, J.G., 1999. Sea Fish. Scandinavian Fishing Yearbook. Hedehusene, Denmark, p. 340. ISBM 87, -90787-00-5.

Pauly, D., Piroddi, C., Hood, L., Bailly, N., Chu, E., Lam, V., Pakhomov, E.A., et al., 2021. The biology of mesopelagic fishes and their catches (1950–2018) by commercial and experimental fisheries. J. Mar. Sci. Eng. 9, 1057. https://doi.org/10.3390/jmse9101057.

Polet, H., 2000. Codend and whole trawl selectivity of a shrimp beam trawl used in the North Sea. Fish. Res. 48, 167–183. https://doi.org/10.1016/S0165-7836(00)00125-9.

Prellezo, R., 2019. Exploring the economic viability of a mesopelagic fishery in the Bay of Biscay. ICES (Int. Counc. Explor. Sea) J. Mar. Sci. 76, 771–779. https://doi.org/10.1093/icesjms/fsy001.

R Core Team, 2020. A Language and Environment for Statistical Computing. R Foundation for Statistical Computing, Vienna, Austria. https://www.R-project.org/.

Santos, J., Herrmann, B., Stepputtis, D., Günther, C., Limmer, B., Mieske, B., Schultz, et al., 2018. Predictive framework for codend size selection of brown shrimp (*Crangon crangon*) in the North Sea beam-trawl fishery. PLoS One. https://doi.org/10.1371/journal.pone.0200464.

Sigurdsson, T., 2017. Mesopelagic Fish: the Icelandic Case. North Atlantic Seafood Forum 2017. Bergen 07 March 2017. http://issuu.com/oktan/docs/annonse2017_final.

Standal, D., Grimaldo, E., 2020. Institutional nuts and bolts for a mesopelagic fishery in Norway. Mar. Pol. 119, 104043 https://doi.org/10.1016/j.marpol.2020.104043, 2020.

Underwood, M.J., Rosen, S., Engås, A., Hemnes, T., Melle, W., Aasen, A., 2016. Flume Tank Testing of a Multiple Inner-Paneled Trawl to Reduce Loss and Clogging of Small Organisms. Cruise Report. Institute of Marine Research, Bergen, Norway. https://www.hi.no/resources/publikasjoner/rapport-fra-havforskningen/2016/flume_tank_report_v4.pdf.

Underwood, M., García-Seoane, E., Klevjer, T.A., Macaulay, G.J., Melle, W., 2020. An acoustic method to observe the distribution and behaviour of mesopelagic organisms in front of a trawl. Deep Sea Res. Part II Top. Stud. Oceanogr. 180, 104873 https://doi.org/10.1016/j.dsr2.2020.104873.

Valdemarsen, J.W., 2001. Technological trends in capture fisheries. Ocean Coast Manag. 44, 635–651. https://doi.org/10.1016/S0964-5691(01)00073-4.

Wickham, H, 2016. ggplot2: Elegant Graphics for Data Analysis. Springer Verlag, New York.

Wileman, D.A., Ferro, R.S.T., Fonteyne, R., Millar, R.B. (Eds.), 1996. Manual of Methods of Measuring the Selectivity of Towed Fishing Gears. ICES Cooperative Research Report No, p. 215.

Xu, P.X., Xu, L.X., Meng, T., Huang, H.L., Zhang, X., Zhou, A.Z., Li, L.Z., Xu, G.D., 2015. Comparative analysis on the performance of Japan and South Korea Antarctic krill mid-water trawls with small mesh sizes. J. Fish. Sci. China 22 (4), 837–846 (in Chinese with English abstract). http://caod.oriprobe.com/articles/46253347/Comparative_analysis_on_the_performance_of_Japan_and_South_Korea_Antar.htm.

Zhou, Aizhong, Chunlei, Feng, Zhang, Xun, et al., 2016. Experiment and research of krill trawl net. Mar. Fish. 38 (1), 74–82 (In Chinese with English abstract).